

# UC San Diego

## UC San Diego Previously Published Works

### Title

Shearing Behavior of Tire-Derived Aggregate with Large Particle Size. II: Cyclic Simple Shear

### Permalink

<https://escholarship.org/uc/item/1zd753gs>

### Journal

Journal of Geotechnical and Geoenvironmental Engineering, 143(10)

### ISSN

1090-0241

### Authors

McCartney, John S  
Ghaaowd, Ismaail  
Fox, Patrick J  
[et al.](#)

### Publication Date

2017-10-01

### DOI

10.1061/(asce)gt.1943-5606.0001781

Peer reviewed

1     **SHEARING BEHAVIOR OF TIRE DERIVED AGGREGATE WITH LARGE PARTICLE**  
2                     **SIZE. II: CYCLIC SIMPLE SHEAR**

3  
4             **by John S. McCartney, Ph.D., P.E., M.ASCE<sup>1</sup>, Ismaail Ghaaowd, M.S., S.M. ASCE<sup>2</sup>,**  
5                     **Patrick J. Fox, Ph.D., P.E., F.ASCE<sup>3</sup>, Michael J. Sanders, M.S., S.M. ASCE<sup>4</sup>,**  
6                     **Stuart S. Thielmann, M.S. <sup>5</sup>, and Andrew C. Sander, M.S., S.M.ASCE<sup>6</sup>**

7  
8     **ABSTRACT:** Although Tire-Derived Aggregate (TDA) has been used widely as lightweight fill  
9 in civil engineering applications, the properties governing its response under cyclic loading are  
10 not well understood. Reliable data on the evolution of shear modulus and damping ratio with  
11 cyclic shear strain amplitude are needed for the prediction of the seismic response of TDA fills,  
12 especially those with larger particle sizes up to 300 mm (Type B TDA). This study presents the  
13 results of cyclic simple shear tests performed on Type B TDA using a new large-scale testing  
14 device for vertical stresses ranging from 19.3 to 76.6 kPa and shear strain amplitudes ranging  
15 from 0.1% to 10%. The shear modulus of Type B TDA has a maximum value of 3,355 kPa and  
16 decreases with increasing shear strain amplitude, which is smaller in magnitude and similar in  
17 trend to natural granular soils in this vertical stress range. Continuous volumetric contraction was  
18 observed during cyclic loading for all stress levels. The damping ratio for Type B TDA showed a  
19 different behavior from granular soils, with a relatively high magnitude of 20 to 25% at the  
20 lowest shear strain amplitude (0.1%), followed by a decreasing/increasing trend with increasing  
21 amplitude. The shear modulus was found to follow a power law relationship with vertical stress,  
22 similar to granular soils, and the damping ratio was not sensitive to vertical stress level.

23

---

<sup>1</sup> Associate Professor, Dept. of Structural Eng., Univ. of California San Diego, 9500 Gilman Dr., La Jolla, CA 92093-0085; mccartney@ucsd.edu

<sup>2</sup> Doctoral Candidate, Dept. of Structural Eng., Univ. of California San Diego, 9500 Gilman Dr., La Jolla, CA 92093-0085; ighaaowd@eng.ucsd.edu

<sup>3</sup> Shaw Professor and Head, Dept. of Civil and Environmental Engineering, The Pennsylvania State University, 212 Sackett Building, University Park, Pa 16802-1408; pjfox@enr.psu.edu

<sup>4</sup>Structural Engineer, Dept. of Structural Eng., Univ. of California San Diego, 9500 Gilman Dr., La Jolla, CA 92093-0085; mjsander@eng.ucsd.edu

<sup>5</sup>Staff Geotechnical Engineer, GeoEngineers, Inc., 1101 S Fawcett Ave # 200, Tacoma, WA 98402

<sup>6</sup>Structural Designer, WRK Engineers, 215 W 12th St #202, Vancouver, WA 98660

24 **INTRODUCTION**

25 The recycling of waste tires in the form of Tire-Derived Aggregate (TDA) as a lightweight  
26 backfill is promoted throughout the U.S., and is particularly important for states that have high  
27 rates of generation, like in California where 40 million tires are discarded every year  
28 (CalRecycle 2016a). TDA with large particle sizes up to 300 mm, referred to as Type B TDA  
29 (ASTM D6270), can be used in layers with a thickness up to 3 m for applications such as  
30 highway embankments or retaining walls (Geosyntec 2008; Ahn et al. 2014; CalRecycle 2016b).  
31 Under static loading, these systems have been shown to have comparable or superior  
32 performance to similar systems constructed with natural backfill soil (Humphrey et al. 1993;  
33 Bosscher et al. 1993; Bosscher et al. 1997; Hoppe 1998; Tweedie et al. 1998; Dickson et al.  
34 2001; Tandon et al. 2007); however, they may also experience strong shaking in seismically-  
35 active regions such as California.

36 The seismic performance of retaining walls constructed with TDA has been evaluated in  
37 large-scale experiments recently by Xiao et al. (2012) and Ahn and Cheng (2014), who found  
38 that TDA has a softer response than natural granular soils and advantageous seismic  
39 characteristics such as lower dynamic earth pressures and the ability to experience large residual  
40 deformations without catastrophic failure. However, these studies did not report TDA cyclic  
41 shear properties that are needed to simulate seismic performance, such as variation of shear  
42 modulus and damping ratio with cyclic strain magnitude under different stress conditions.  
43 Although there have been studies on the cyclic properties of TDA with relatively small particle  
44 sizes mixed with natural soils (Bosscher et al. 1997; Feng and Sutterer 2000; Kaneko et al. 2003;  
45 Anastasiadis et al. 2012a, 2012b; Senetakis et al. 2012a, 2012b, Nakhei et al. 2012; Mashiri et al.  
46 2013; Ehsani et al. 2015), the cyclic properties of Type B TDA have not been evaluated due to

47 the need for a large testing device to accommodate the large particle size. There are also other  
48 applications where TDA may experience cyclic loading, such as a cushion material to dampen  
49 vibrations from compaction (Lee and Roh 2007), a coastal liquefaction mitigation measure  
50 (Hazarika et al. 2008), and a seismic isolation layer for building foundations (Tsang 2008).  
51 Accordingly, more data and information are needed on the dynamic properties of Type B TDA  
52 for earthquake engineering design.

53 To address this need, Fox et al. (2017) developed a novel large-scale combination direct  
54 shear/simple shear device for Type B TDA that can accommodate specimens measuring 3048  
55 mm  $\times$  1219 mm in plan and up to 1830 mm in height. This paper presents the results of cyclic  
56 simple shear tests on Type B TDA material using this device. The data include shear modulus,  
57 damping ratio, and volumetric strain under a range of vertical stresses and cyclic shear strain  
58 amplitudes. A companion paper (Ghaaowd et al. 2017) presents corresponding data for TDA  
59 internal direct shear and TDA-concrete interface direct shear tests obtained using the same  
60 device.

## 61 **BACKGROUND**

62 Feng and Sutterer (2000) noted several characteristics of granulated rubber from waste tires  
63 that make the dynamic response potentially different from natural soils, including elastic  
64 behavior over a wider range of deformation, a relatively ductile stress-strain curve, and more  
65 extensive recovery from large deformations when stresses are removed. Further, the granulated  
66 rubber particles have a lower modulus of elasticity than soil particles, and have a Poisson's ratio  
67 of nearly 0.5 indicating low volume compressibility.

68 Three previous studies investigated the cyclic response of TDA, as described in Table 1.  
69 Feng and Sutterer (2000) performed resonant column tests to measure the shear modulus and

70 damping ratio of granulated rubber (particle size = 2.00 to 4.76 mm) mixed with Ottawa sand,  
71 and found that the addition of sand produced an increase in shear modulus and reduction in  
72 damping ratio. They also tested pure granulated rubber and measured shear modulus values  
73 ranging from 1100 to 2800 kPa for effective stresses ranging from 69 to 483 kPa and shear  
74 strains ranging from 0.003 to 0.1%. This range of effective stress is much greater than expected  
75 for many TDA construction applications, such as retaining walls or embankments, and thus  
76 additional work is needed to understand variations in shear modulus at lower effective stress  
77 levels. Feng and Sutterer (2000) also observed that damping ratio of granulated rubber was not  
78 particularly sensitive to effective stress, and had an initially high value of 4.5 to 6.0%. In most of  
79 their tests, the damping ratio increased with increasing shear strain amplitude, while in one test a  
80 small decrease was observed initially followed by an increase at higher shear strain amplitudes.

81 Kaneko et al. (2003) performed cyclic shear strain tests on saturated specimens of TDA in  
82 the form of tire chips having a maximum particle size of 1.1 mm. The measured hysteresis loops  
83 have shapes similar to those for natural soils, with a clear peak value at the point of strain  
84 reversal. Kaneko et al. (2003) also found that, because the particles are deformable, shear strains  
85 can be accommodated with less particle sliding and rearrangement. This feature, combined with  
86 the high hydraulic conductivity, suggests that tire chips will not experience generation of excess  
87 pore water pressures during cyclic loading that may lead to liquefaction. The hysteresis loops  
88 reported by Kaneko et al. (2003) were reinterpreted by the authors to calculate shear modulus  
89 and damping ratio for different effective stress values, which are reported in Table 1. Hazarika et  
90 al. (2010) performed a cyclic simple shear tests on a saturated specimen of TDA in the form of  
91 tire chips having a maximum particle size of 1.0 mm. The hysteresis loop for this test was

92 reinterpreted by the authors to define the shear modulus and damping ratio, which are reported in  
93 Table 1.

94 Several studies have investigated the shear modulus and damping ratio of soil-TDA mixtures  
95 (Feng and Sutterer 2000; Kaneko et al. 2003, Anastasiadis et al. 2012a, 2012b; Senetakis et al.  
96 2012a, 2012b, Nakhei et al. 2012; Mashiri et al. 2013; Ehsani et al. 2015). These studies  
97 generally observed that the shear modulus decreased and the damping ratio increased with the  
98 percentage of TDA in the soil-TDA mixture. For example, Anastasiadis et al. (2012a) found that  
99 the shear modulus decreased from 45 to 10 MPa and the damping ratio increased from 0.68 to  
100 0.40% when adding 35% TDA to soil at a confining stress of 30 kPa.

101 Although the resilient modulus is not as useful as the shear modulus versus cyclic shear  
102 strain relationship, studies on resilient modulus may provide further insight into the cyclic  
103 response of TDA. Bosscher et al. (1997) evaluated the resilient modulus of TDA having a  
104 maximum particle size of 75 mm, and found that the cyclic loading force-displacement hysteresis  
105 loops and resulting modulus of subgrade reaction values do not change significantly from the  
106 first cycle with continued cyclic loading. Values of resilient modulus increased from 1000 to  
107 1900 kPa as the effective confining stress increased from 19 to 105 kPa. The subgrade reaction  
108 experimental design in the Bosscher et al. (1997) study did not allow for measurement of shear  
109 modulus and damping ratio values, or control of shear strain amplitude, and thus the results are  
110 limited in terms of TDA dynamic properties. The specimen size in these tests was also limited  
111 and could not accommodate large-size TDA material.

112 Two recent studies have evaluated the seismic response of TDA used as a backfill in gravity  
113 retaining walls (Ahn and Cheng 2014) and geosynthetic-reinforced retaining walls (Xiao et al.  
114 2012). Ahn and Cheng (2014) performed a shake table test on a large-scale (2 m high) cantilever

115 retaining structure constructed from a layer of Type B TDA and an overlying layer of sand, and  
116 found that the dynamic pressure exerted on the wall was smaller in the TDA layer. Further, the  
117 TDA experienced relatively large residual shear deformations of up to 50 mm without  
118 catastrophic failure. Xiao et al. (2012) performed a shake table test on a reduced-scale (1.6 m  
119 high) geosynthetic-reinforced retaining structure constructed from TDA with a maximum  
120 particle size of 150 mm, and compared the results with a similarly-constructed wall using only  
121 sand. The wall constructed with TDA backfill had less lateral displacement, less vertical  
122 settlement, apparent acceleration attenuation toward the top of the wall, and lower static and  
123 dynamic lateral stresses on the wall. These studies indicate that TDA backfill for retaining walls  
124 offers several advantages in comparison to natural backfill soils.

## 125 **EXPERIMENTAL EQUIPMENT AND PROCEDURES**

### 126 **Equipment**

127 A schematic diagram and photograph of the large-scale combination direct shear/simple  
128 shear device developed by Fox et al. (2017) are shown in Figure 1. The inside dimensions of the  
129 shearing box in simple shear mode are 3048 mm  $\times$  1219 mm in plan, with a height of 1600 mm.  
130 The specimen height used for the simple shear tests is approximately 1400 mm, which is shorter  
131 than the specimen height used in direct shear mode. The sides of the box in the direction parallel  
132 to shear consist of stacked tubular steel members, while the sides of the box in the direction  
133 perpendicular to shear consist of vertical solid steel plates. In the simple shear mode, the tubular  
134 members are pinned to the steel plates on the ends so that the box can deform as a parallelogram  
135 and induce shear strain to the TDA specimen. Two hydraulic actuators are used to provide the  
136 horizontal force and are operated in displacement-control mode. The actuator stroke allows the  
137 box to be cycled in either direction with a maximum shear strain of 30%. The horizontal

138 displacement  $\Delta x$  is measured on the top of the device at a height of  $H = 1600$  mm using a string  
139 potentiometer, which is needed to calculate the shear strain  $\gamma (= \Delta x/H)$ . Transverse fins on the top  
140 and bottom surfaces of the box (i.e., above and below the specimen) are used to minimize  
141 slippage of the TDA specimen and increase the uniformity of shear stress application.  
142 Instrumentation includes a load cell for each actuator, four potentiometers (i.e., one at each  
143 corner of the box) to measure vertical displacements, a string potentiometer to measure  
144 horizontal displacements, and tiltmeters to measure vertical end plate and actuator rotations.  
145 Eight load cells were placed between the top plate and the TDA to measure uniformity of contact  
146 stress during the shearing process. The load cell measurements were nearly identical throughout  
147 shearing. Additional details regarding design and evaluation of the device are provided by Fox et  
148 al. (2017) and the companion paper (Ghaaowd et al. 2017).

## 149 **Procedures**

150 The Type B TDA material and specimen preparation procedures for the current study were  
151 the same as for the direct shear testing program described in the companion paper (Ghaaowd et  
152 al. 2017). Plastic sheeting was used to line the inside walls of the box to reduce sidewall friction,  
153 and the TDA was compacted in 100 mm-thick loose lifts using a 14.4 kN rolling and vibrating  
154 compactor and 6 passes per lift. Although the compactor weight is lower than that suggested in  
155 ASTM D6270 (90 kN), the lift thickness used in this study is smaller, and the lateral constraint  
156 provided by the box may lead to greater densities than expected in the field for the same  
157 compaction energy (Ghaaowd et al. 2017).

158 The testing program is summarized in Table 2 and consisted of four simple shear tests, SS1  
159 to SS4, each conducted using a single TDA specimen to characterize the effects of vertical stress  
160 ( $\sigma = 19.3$  to  $76.6$  kPa) and cyclic shear strain amplitude ( $\gamma_a = 0.1$  to  $10\%$ ) on secant shear



161 modulus and damping ratio. Each test included multiple stages, with each stage consisting of 20  
162 cycles of back-and-forth shearing under constant applied stress and using a triangular waveform  
163 with constant shear strain amplitude and constant actuator displacement rate of 16 mm/min. At  
164 the elevation of the string potentiometer (1600 mm), this corresponds to a displacement rate of  
165 24 mm/min and a shear strain rate of 1.5%/min. Displacement rates for the simple shear tests are  
166 sufficiently slow that inertial forces are negligible and have no effect on the measured results.  
167 Tests SS2, SS3, and SS4 included five stages of progressively increasing shear strain amplitude  
168 ( $\gamma_a = 0.1, 0.3, 1, 3, \text{ and } 10\%$ ), and test SS1 included eight stages also spanning between  $\gamma_a = 0.1\%$   
169 and 10%, with one reversal in between (Table 2). The tests were operated in displacement-  
170 control mode with shearing force measured at the actuators and corrected for actuator tilt from  
171 horizontal. A static waiting period of 30 minutes (i.e.,  $\gamma = 0$ ) was included between the  
172 successive stages of each test.

## 173 **RESULTS**

174 The total unit weight of TDA after compaction was approximately  $5.6 \text{ kN/m}^3$  for each test.  
175 Dead weight loading increased the total unit weights to the initial values provided in Table 2,  
176 which range from  $5.64$  to  $7.07 \text{ kN/m}^3$  and are consistent with corresponding values for the TDA  
177 direct shear tests (Ghaaowd et al. 2017). Further, this range of unit weight values is typical of  
178 TDA used in monolithic fill applications (CalRecycle 2011, 2016b). Using a specific gravity of  
179 1.15 (Ghaaowd et al. 2017), the corresponding values of void ratio range from 1.00 to 0.60. Due  
180 to the relatively large height of TDA specimens in the current study, self-weight of the TDA  
181 material yielded an increase in vertical stress of 9.0 to 11.4 kPa from top to bottom. The  
182 variation of vertical stress across the specimen is much greater than for conventional-sized  
183 simple shear tests, in which soil self-weight is typically ignored, and may have an effect on

184 results when material response varies nonlinearly with effective stress. Vertical stresses in Table  
185 2 and listed in the figures are the values at specimen mid-height.

186 The results from test SS1 are shown in Figure 2. This was the first test performed to  
187 characterize the cyclic simple shear response of Type B TDA, and was different than the other  
188 tests. The shear strain amplitude was increased in stages up to 3%, then decreased in stages to  
189 0.1%, after which the test was stopped. The specimen was then removed and recompacted, the  
190 vertical stress was reapplied, and shearing was started again at  $\gamma_a = 3.0\%$  and then increased to  
191 10%. The horizontal displacement time history for all stages of the test is shown in Figure 2(a).  
192 As the hydraulic actuators were operated in displacement-control mode, reversals occur regularly  
193 within each cycle and amplitude is nearly constant within each stage. The corresponding shear  
194 force values are shown in Figure 2(b). After application of a few cycles, the shear force tends to  
195 stabilize for each stage of the test. However, for some of the cycles at the highest cyclic shear  
196 strain amplitude, slack in the system due to a gap between the top loading plate and the end  
197 plates affected the force values needed to reach the target strain amplitude, as will be observed in  
198 the hysteresis loops for this test (see below). This was corrected in subsequent tests by adding  
199 spacer blocks to close this gap. Volumetric strains during cyclic shearing are shown in Figure  
200 2(c), and indicate continuous contraction and a decreasing rate of contraction with continued  
201 cycling for each stage, similar to natural soils. After recompaction and reloading, the specimen  
202 yielded a force amplitude for  $\gamma_a = 3.0\%$  that was nearly the same as the previous loading at  $\gamma_a =$   
203 3.0%. This indicates good repeatability of cyclic shear results for the same loading conditions.

204 The results from tests SS2, SS3 and SS4 are shown in Figures 3, 4 and 5, respectively, and  
205 display similar behavior for higher vertical stress levels. The actuators indicate good  
206 displacement control, with the exception of one cycle during the final stage of SS2. After a few

207 cycles, the shear force was observed to nearly stabilize during each stage of the tests.  
208 Continuous contraction was observed in all cases, and volumetric strains did not stabilize after  
209 20 cycles for each stage similar to test SS1. This response is consistent with observations for  
210 granular soils. For example, Lee and Albaisa (1974) observed volumetric contraction for both  
211 loose and dense sands during cyclic shear loading, while Hsu and Vucetic (2004) and Whang et  
212 al. (2000) observed similar trends for compacted soils. These studies indicated that more than  
213 100 loading cycles may be needed to reach the equilibrium state for volumetric contraction.  
214 Youd (1972) found that volumetric strain equilibrium was not reached in drained cyclic simple  
215 shear tests on sand after 10,000 cycles, although a progressively slower rate of contraction is  
216 observed with continued cycling.

217 A comparison of the volumetric strains after 20 cycles for each stage of the four tests is  
218 shown in Figure 6. To define the curve for test SS1, values were taken from the first loading  
219 sequence and then from the end of cyclic loading for the 3 and 10% shear strains on the  
220 reloading sequence. Similar to the findings for natural granular soils (e.g., Silver and Seed 1971;  
221 Youd 1972), vertical stress does not have a significant effect on the evolution of volumetric  
222 strain with increasing cyclic shear strain amplitude. It is also interesting that all of the tests  
223 showed volumetric contraction during cyclic shearing regardless of the applied vertical stress or  
224 initial total unit weight. This indicates that, similar to granular soils, the TDA particles continued  
225 to adjust and densify under continuous cycling, but did not ride over each other to cause dilation  
226 as occurred for the corresponding TDA monotonic direct shear tests at large displacements  
227 (Ghaaowd et al. 2017). In the direct shear tests, contraction was observed in each case until the  
228 horizontal displacement was approximately 120-150 mm, after which all specimens exhibited

229 dilation. The amount of this initial contraction increased with the normal stress level, and the  
230 dilation response decreased with increasing normal stress.

## 231 ANALYSIS

232 Shear stresses were calculated by dividing measured shear force by the plan cross-sectional  
233 area of the box and shear strains were calculated by dividing applied horizontal displacement by  
234 the elevation of the displacement measurement ( $H = 1600$  mm). The hysteresis loops for all  
235 stages of each test are shown in Figure 7. The hysteresis loops have a similar shape and are  
236 symmetric about the origin. The size of the hysteresis loops increases with increasing vertical  
237 stress, and at higher stress levels the loops for tests SS3 and SS4 are more consistent in shape  
238 than for tests SS1 and SS2. The slack in the system in test SS1 is reflected in the change in shape  
239 near the strain limits at the highest cyclic shear strain amplitude in Figure 7(a). Data from these  
240 loops were not included in the subsequent analysis of TDA secant shear modulus and damping  
241 ratio.

242 The backbone curves for the four tests are shown in Figure 8. Each curve was prepared by  
243 plotting the maximum shear stress against corresponding shear strain amplitude for the final (i.e.,  
244 20<sup>th</sup>) cycle of loading at each test stage. The curves display nonlinearity with increasing shear  
245 strain and are symmetric about the origin similar to the hysteresis loops. An increase in  
246 magnitude of the shear stress with increasing vertical stress is also observed, as expected.  
247 Interestingly, even at 10% shear strain, the TDA has still not reached a peak shear strength value.  
248 This is in contrast to dense sands, which would generally be expected to reach peak strength by  
249 this point (Lee and Seed 1967). Values of secant shear modulus were calculated from the peak  
250 end points of the hysteresis loops, as follows:

$$G = G_{secant} = \frac{(\tau_{max} - \tau_{min})}{(\gamma_{max} - \gamma_{min})} \quad (1)$$

251 Values of damping ratio indicate relative energy dissipation during cyclic shearing, and were  
252 calculated on an average basis for the 20 cycles of each testing stage as follows:

$$D = \frac{1}{4\pi} \frac{A_L}{A_T} \quad (2)$$

253 where  $A_L$  is the area within the hysteresis loop, which was calculated using a drafting software,  
254 and  $A_T$  is the area within a right triangle extending from the origin to the peak of the curve,  
255 defined as follows:

$$A_T = \frac{1}{2} \frac{(abs(\tau_{max}) + abs(\tau_{min}))}{2} \frac{(abs(\gamma_{max}) + abs(\gamma_{min}))}{2} \quad (3)$$

256 Values of normalized shear modulus  $G/G_1$  are plotted during cyclic loading for each stage  
257 (i.e., each  $\gamma_a$ ) of test SS3 in Figure 9(a), where  $G$  is the shear modulus for each cycle and  $G_1$  is  
258 the shear modulus for the first cycle of loading. The normalized shear modulus increases  
259 gradually throughout each stage as a result of continuing volumetric contraction (Fig. 4c). The  
260 normalized damping ratio  $D/D_1$  is plotted similarly in Figure 9(b), where  $D$  is the damping ratio  
261 for each cycle and  $D_1$  is the damping ratio for the first cycle of loading. For each stage, values  
262 slightly decrease and then approach a relatively stable value at high number of cycles. Similar  
263 trends were observed for the other tests.

264 Representative values of shear modulus and damping ratio were calculated for each test stage  
265 as an average over the last five cycles. In the few cases where slack in the system affected the  
266 hysteresis loops, the peaks of unaffected hysteresis loops were used to obtain the average shear  
267 modulus and damping ratio. Figure 10(a) presents the shear modulus reduction curve (i.e.,  $G$  vs.  
268  $\log \gamma_a$ ) for each test. Similar to natural soils, shear modulus decreases nonlinearly with increasing  
269 shear strain amplitude for each vertical stress. The testing program did not include, and the  
270 device may not be capable of producing, very low shear strain levels associated with the small

271 strain shear modulus  $G_{max}$ . Figure 10(a) also shows that shear modulus increases with increasing  
272 vertical stress for each cyclic shear strain amplitude. Despite the difference in strain history, the  
273 data from test SS1 follows a consistent trend with the other three tests. The secant shear modulus  
274 of Type B TDA ranges from 200 to 3355 kPa, which is similar in order of magnitude to values  
275 reported in Table 1 for tire chips and granulated rubber with smaller particle sizes at similar  
276 cyclic shear strain amplitudes (Feng and Sutterer 2000; Kaneko et al. 2003; Hazarika et al.  
277 2010).

278 A corresponding plot of damping ratio vs. cyclic shear strain amplitude is shown in  
279 Figure 10(b). At the smallest amplitude (0.1%), damping ratio ranges from 21% to 24% and is  
280 greater than typical values for natural granular soils at similar amplitudes, which might be  
281 expected to range from approximately 5 to 20% (e.g., Seed and Idriss 1970; Seed et al. 1986;  
282 Rollins et al. 1998). Damping ratio decreases and then increases with increasing  $\gamma_a$  for each test,  
283 and shows close agreement for all four vertical stress levels. The shape of the relationships in  
284 Figure 10(b) is similar to that reported for one of the tests on granulated rubber conducted by  
285 Feng and Sutterer (2000) at a confining stress of 345 kPa (the other tests in that study showed  
286 consistently increasing damping ratio). A comparison of the damping ratios from the previous  
287 studies listed in Table 1 indicates that the magnitudes reported by Feng and Sutterer (2000) were  
288 smaller ( $\leq 6\%$ ) but the strain ranges under investigation were much smaller. The damping ratios  
289 obtained from a reinterpretation of the data from Kaneko et al. (2003) and Hazarika et al. (2010)  
290 reported in Table 1 have similar magnitudes as those observed in the current study because their  
291 cyclic strain amplitudes were on the same order of magnitude as in this study. Interestingly, the  
292 decreasing/increasing trend in Fig. 10(b) is similar to the trend shown by Nye and Fox (2007) for  
293 cyclic shear tests on a hydrated needle-punched geosynthetic clay liner (GCL).

294 An evaluation of the repeatability of the shear modulus and damping ratio values obtained  
295 from the application of the same cyclic shear strain magnitudes to different specimens in test SS1  
296 is shown in Figure 11. Despite the different specimens, which may have had slightly different  
297 structure and density, values of shear modulus and damping ratio are in close agreement at each  
298 strain amplitude.

299 Variation of shear modulus with vertical stress for all four tests is presented in Figure 13.  
300 Although values at the smallest cyclic shear strain amplitude of 0.1% do not correspond to small  
301 strains, these values follow a trend with vertical stress that is similar to the power law  
302 relationship of Hardin and Black (1966), which can be expressed as follows, neglecting the  
303 effects of void ratio and overconsolidation ratio:

$$G = A \left( \frac{\sigma_v}{P_{atm}} \right)^n \quad (4)$$

304 where  $\sigma_v$  is the vertical normal stress,  $P_{atm}$  is the atmospheric pressure (101.3 kPa), and  $A$  and  $n$   
305 are fitting parameters. Best-fit curves and the corresponding equations, as obtained using Eq. (4)  
306 with nonlinear regression, are also show in Figure 13. Close agreement is observed for each  
307 shear strain amplitude for Type B TDA, with  $n$  values ranging from 0.48 to 0.71 and increasing  
308 with increasing strain amplitude. The value of  $n$  is typically assumed to be 0.5 for granular soils,  
309 and the parameters in Figure 12 indicate that this assumption may also be suitable for Type B  
310 TDA except for the two highest shear strain amplitudes where higher  $n$  values are needed..

311 Although sufficiently small cyclic shear strain amplitudes were not applied to measure  $G_{max}$   
312 in the current study, the value of  $G_{max}$  may be inferred by fitting established shear modulus  
313 reduction curves to the data in Figure 10(a). The model of Darandeli (2001) was used and is  
314 described as follows:

$$\frac{G}{G_{max}} = \left( \frac{1}{1 + \left( \frac{\gamma}{\gamma_r} \right)^a} \right) \quad (5)$$

315 where  $a$  is a fitting parameter,  $\gamma_r$  is a threshold shear strain, and  $G_{max}$  is assumed to follow the  
 316 same trend with vertical normal stress given by Equation (4). Darandeli (2001) proposed an  
 317 empirical equation to estimate the value of  $\gamma_r$  for granular soils, but the calculated values were  
 318 too small to fit the experimental data in Figure 10(a). Accordingly, the following power law  
 319 equation was used to characterize the effects of vertical normal stress on  $\gamma_r$ :

$$\gamma_r = \gamma_0 \left( \frac{\sigma_v}{P_{atm}} \right)^m \quad (6)$$

320 The values of  $A$  in Equation (4),  $a$  in Equation (5), and  $\gamma_0$  and  $m$  in Equation (6) were varied to  
 321 obtain the best fit to the experimental data in Figure 10(a), and the resulting modulus reduction  
 322 curves using  $A = 5100$  kPa,  $a = 0.80$ ,  $\gamma_0 = 0.6$ , and  $m = 0.55$  are shown in Figure 13(a) and 13(b)  
 323 in terms of the shear modulus and the normalized shear modulus  $G/G_{max}$ , respectively. Although  
 324 some discrepancy is noted, the model provides a reasonable overall fit to the experimental data  
 325 for Type B TDA. An alternative approach would be to measure the small-strain shear modulus in  
 326 the laboratory or field using a wave propagation technique, and then modify the shear modulus  
 327 trends reported in the current study to estimate project-specific modulus reduction curves.

328 For comparison, the results from Stokoe et al. (1994) can be used to estimate the shear  
 329 modulus of compacted sand at a similar stress state as that evaluated for Type B TDA. Stokoe et  
 330 al. (1994) observed that the shear modulus of remolded sand decreases about 40% from the value  
 331 at small strain to the value at  $\gamma_a = 0.1\%$ . The shear modulus of sand at a confining stress of 80  
 332 kPa and  $\gamma_a = 0.1\%$  is approximately 32000 kPa, which is about 10 times larger than the highest  
 333 value observed for Type B TDA in the current study. Stokoe et al. (1994) also reported that the



334 damping ratio increased by about 10 times during application of cyclic shear strains from small  
335 strain up to 0.1%. Considering the minimum damping ratio for sands at a confining stress of  
336 80 kPa is approximately 0.6%, the damping ratio at  $\gamma_a = 0.1\%$  is expected to be approximately  
337 6%. This is much smaller than the values calculated for Type B TDA. As such, TDA may not  
338 have as high of a shear modulus as compacted sands, but has much higher damping. Thus, Fills  
339 made of Type B TDA may experience greater displacements than granular soils during seismic  
340 events, and also may dissipate more energy depending on the frequency content of the motion  
341 and the fundamental mode of the structure.

## 342 **CONCLUSIONS**

343 Large-scale cyclic simple shear tests were conducted to measure and better understand the  
344 cyclic properties and behavior of Type B Tire Derived Aggregate (TDA) with large particle size.  
345 The cyclic simple shear tests were performed for vertical stresses ranging from 19.3 to 76.6 kPa  
346 and shear strain amplitudes ranging from 0.1% to 10%. The observed shear stress-shear strain  
347 hysteresis loops were similar to those of granular soils, with a lower shear modulus and a  
348 significantly larger damping ratio. The shear modulus of Type B TDA has a maximum value of  
349 3,355 kPa and decreases with increasing shear strain amplitude, which is smaller in magnitude  
350 and similar in trend to natural granular soils in this vertical stress range. Similar to granular soils,  
351 the shear modulus increased nonlinearly with increasing vertical stress following a power law  
352 relationship. The damping ratio for Type B TDA showed a different behavior from granular  
353 soils, with a relatively high magnitude of 20 to 25% at the lowest shear strain amplitude (0.1%),  
354 followed by a decreasing/increasing trend with increasing amplitude. The damping ratio was  
355 essentially independent of the vertical stress level. Continuous contraction of the Type B TDA  
356 was observed during the cyclic shearing process for all vertical stress levels. The dynamic

357 properties of Type B TDA presented in this paper are the most reliable values yet obtained and  
358 should be useful to avoid the over-conservatism often necessary with assumed parameters.

## 359 **ACKNOWLEDGMENTS**

360 Financial support from California Department of Resources Recycling and Recovery  
361 (CalRecycle) for project DRR11064, and in particular the assistance of Stacey Patenaude and  
362 Bob Fujii of CalRecycle and Joaquin Wright of GHD Consultants, Sacramento, is gratefully  
363 acknowledged. The authors also thank the staff of the Powell Laboratories at UCSD for  
364 assistance with the experimental work. The contents of this paper reflect the views of the authors  
365 and do not necessarily reflect the views of the sponsor.

## 366 **APPENDIX I. REFERENCES**

- 367 Ahn, I., Cheng, L., Fox, P.J., Wright, J., Patenaude, S., and Fujii, B. (2014). “Material properties  
368 of large-size tire derived aggregate for civil engineering applications.” *Journal of Materials in  
369 Civil Engineering*, DOI: 10.1061/(ASCE)MT.1943-5533.0001225, 04014258.
- 370 Ahn, I.-S., and Cheng, L. (2014). “Tire derived aggregate for retaining wall backfill under  
371 earthquake loading.” *Construction and Building Materials*. 57, 105-116.
- 372 American Society for Testing and Materials. (2012) ASTM D6270: Standard Practice for Use of  
373 Scrap Tires in Civil Engineering Applications. ASTM International, West Conshohocken,  
374 PA.
- 375 Anastasiadis, A., Senetakis, K., Pitilakis, K., Gargala, C., and Karakasi, I. (2012a). “Dynamic  
376 behavior of sand/rubber mixtures. Part 1: Effect of rubber content and duration of  
377 confinement on small-strain shear modulus and damping ratio.” *Journal of ASTM  
378 International*. 9(2), 1-19.

379 Anastasiadis, A., Senetakis, K., Pitolakis, K. (2012). “Small strain shear modulus and damping  
380 ratio of sand/rubber and gravel/rubber mixtures.” *Journal of Geotechnical and Geological*  
381 *Engineering*. 30(2), 363-382.

382 Eldin, (1993). “Construction and performance of shredded waste tire test embankment.”  
383 *Transportation Research Record*. Transportation Research Board, Washington, DC. Volume  
384 1345, 44-52.

385 Bosscher, P.J., Edil, T.B., and Kuraoka, S. (1997). “Design of highway embankments using tire  
386 chips.” *Journal of Geotechnical and Geoenvironmental Engineering*. 123(4), 295-304.

387 CalRecycle. (2016a). *California Waste Tire Market Report: 2015*. Publication # DRRR 2016-  
388 01567. Sacramento, CA.

389 CalRecycle. (2016b). *Usage Guide: Tire-Derived Aggregate (TDA)*. Publication # DRRR 2016-  
390 01545. Sacramento, CA.

391 CalRecycle. (2011). *Civil Engineering Applications Using Tire Derived Aggregate (TDA)*.  
392 Publication # DRRR-2011-038. Sacramento, CA.

393 Darendeli, M.B. (2001). *Development of a New Family of Normalized Modulus Reduction and*  
394 *Material Damping Curves*. PhD Dissertation, Univ. of Texas. Austin, Tex.

395 Dickson, T.H., Dwyer, D.F., Humphrey, D.N. (2001). “Prototype tire-shred embankment  
396 construction.” *Transportation Research Record*, 1755, National Research Council,  
397 Transportation Research Board, Washington, D.C. pp. 160-167.

398 Edil, T.B. and Bosscher, P.J. (1994). “Engineering properties of tire chips and soil mixtures.”  
399 *Geotechnical Testing Journal*, 17(4), 453-464.

400 Ehsani, M., Shariatmadari, N., Mirhosseini, S.M. (2015). “Shear modulus and damping ratio of  
401 sand-granulated rubber mixtures.” *J. Cent. South Univ.* 22, 3159–3167.

402 Feng, Z.Y. and Sutterer, K.G. (2000). “Dynamic properties of granulated rubber/sand mixtures.”  
403 ASTM Geotechnical Testing Journal. 23(3), 338–344.

404 Fox, P.J., Sanders, M., Latham, C., Ghaaowd, I., and McCartney, J.S. (2017). “Large-scale  
405 direct-simple shear test for large-particle tire-derived aggregates.” ASTM Geotechnical  
406 Testing Journal. Accepted.

407 Geosyntec. (2008). Guidance Manual for Engineering Uses of Scrap Tires. Prepared for  
408 Maryland Department of the Environment. Geosyntec Project No.: ME0012-11.

409 Ghaaowd, I., McCartney, J.S., Thielmann, S.S., Sanders, M.J., and Fox, P.J. (2017). “Shearing  
410 behavior of tire derived aggregate with large particle size. I. Internal and concrete interface  
411 direct shear.” Journal of Geotechnical and Geoenvironmental Engineering. Companion  
412 paper.

413 Hardin, B.O. and Black, W.L. (1966). “Sand stiffness under various triaxial stresses. ASCE  
414 Journal of the Soil Mechanics and Foundation Division. 92(SM2), 27-42.

415 Hazarika, H., Yasuhara, K., Kamokar, A.K., and Mitarai, Y. (2008). “Shaking table test on  
416 liquefaction prevention using tire chips and sand mixture.” In: Hazarika H, Yasuhara K,  
417 editors. International Workshop on Scrap Tire Derived Geomaterials: Opportunities and  
418 Challenges. Taylor and Francis. 215–22.

419 Hazarika, H., Kohama, E., and Sugano, T. (2008). “Underwater shake table tests on waterfront  
420 structures protected with tire chips cushion.” Journal of Geotechnical and Geoenvironmental  
421 Engineering. 134(12), 1706–1719.

422 Hazarika, H., Hyodo, M., and Yasuhara, K. (2010). “Investigation of tire chips-sand mixtures as  
423 preventative measure against liquefaction.” GeoShanghai 2010. ASCE. 338-345.

424 Hoppe, E.J. (1998). "Field study of shredded-tire embankment," Transportation Research Record  
425 No. 1619, Transportation Research Board, Washington, DC. 47-54.

426 Hsu, C., Vucetic, M. (2004). "Volumetric threshold shear strain for cyclic settlement." Journal of  
427 Geotechnical and Geoenvironmental Engineering. 130(1), 58-70

428 Humphrey, D., Sandford, T., Cribbs, M., and Manion, W. (1993). "Shear strength and  
429 compressibility of tire chips for use as retaining wall backfill." Transportation Research  
430 Record. Transportation Research Board, Washington, DC. Volume 1422, 29-35.

431 Kaneko, T., Orense, R.P., Hyodo, M., and Yoshimoto, N. (2003). "Seismic response  
432 characteristics of saturated sand deposits mixed with tire chips." Journal of Geotechnical and  
433 Geoenvironmental Engineering. 139(4), 633-643.

434 Lee, K.L., and Albaisa, A. (1974). "Earthquake induced settlements in saturated sands." Journal  
435 of the Geotechnical Engineering Division. ASCE, 103(6), 535-547.

436 Lee, H.J. and Roh, H.S. (2007). "The use of recycled tire chips to minimize dynamic earth  
437 pressure during compaction of backfill." Construction and Building Materials. 21, 1016-  
438 1026.

439 Lee, K.L., and Seed, H.B. (1967). "Drained strength characteristics of sands." Journal of the Soil  
440 Mechanics and Foundation Division. SM6, 118-143.

441 Mashiri, M.S., Sheikh, M., Neaz., V.J. and Tsang, H. (2013). "Dynamic properties of sand-tyre  
442 chip mixtures." Australian Earthquake Engineering Society Conference. S. Anderson, Ed.  
443 Australian Earthquake Engineering Society, Tasmania. 1-8.

444 Nakhaei, A. Marandi, S.M., Sani Kermani, S., Bagheripour, M.H. (2012). "Dynamic properties  
445 of granular soil mixed with granulated rubber." Soil Dynamics and Earthquake Engineering.  
446 43, 124-232.

447 Nye, C.J., and Fox, P.J. (2007). "Dynamic shear behavior of a needle-punched geosynthetic clay  
448 liner." *Journal of Geotechnical and Geoenvironmental Engineering*. 133(8), 973-983.

449 Rollins, K.M., Evans, M., Diehl, N., and Daily, W. (1998). "Shear modulus and damping  
450 relationships for gravels." *Journal of Geotechnical and Geoenvironmental Engineering*.  
451 124(5), 396-405.

452 Seed, H.B., and Idriss, I.M. (1970). "Soil moduli and damping factors for dynamic response  
453 analysis." Rep. No. EERC 70-10, Earthquake Engineering Research Center, Berkeley, Calif.

454 Seed, H.B., Wong, R.T., Idriss, I.M., and Tokimatsu, K. (1986). "Moduli and damping factors  
455 for dynamic analyses of cohesionless soils." *Journal of Geotechnical Engineering*. 112(11),  
456 1016-1032.

457 Senetakis, K., Anastasiadis, A., Pitilakis, K., Souli, A. (2012a). "Dynamic behavior of  
458 sand/rubber mixtures, Part II: Effect of rubber content on G/G<sub>0</sub>-c-DT curves and volumetric  
459 threshold strain. *Journal of ASTM International*, 9(12), 1-12.

460 Senetakis, K., Anastasiadis, A., Pitilakis, K. (2012b). "Dynamic properties of dry sand/rubber  
461 (SRM) and gravel/rubber (GRM) mixtures in a wide range of shearing strain amplitudes."  
462 *Soil Dynamics and Earthquake Engineering*. 33, 38-53.

463 Silver, M.L., and Seed, H.B. (1971). "Volume changes in sands during cyclic loading." *Journal*  
464 *of Soil Mechanics and Foundations Division*. 97(SM9), 1171-1182.

465 Stokoe, K.H., III, Hwang, S. K., and Lee, J. N.-K., and Andrus, R. (1995). "Effects of various  
466 parameters on the stiffness and damping of soils at small to medium strains." *Proceedings of*  
467 *1st International Symp. On Pre-failure Deformation Characteristics of Geomaterials*. Vol. 2,  
468 785-816.

469 Tandon, V., Velazco, D.A., Nazarian, S., and Picornell, M. (2007). “Performance monitoring of  
470 embankments containing tire chips: Case study.” *Journal of Performance of Constructed*  
471 *Facilities*. 21(3), 207–214.

472 Whang, D., Riemer, M.F., Bray, J.D., Stewart, J.P., and Smith, P.M. (2000). “Characterization of  
473 seismic-compression of some compacted fills.” *Geo-Denver Conference*, ASCE, Denver,  
474 CO., 180-194.

475 Tsang, H.H. (2008). “Seismic isolation by rubber–soil mixtures for developing countries.”  
476 *Earthquake Engineering and Structural Dynamics*. 37(2), 283–303.

477 Xiao, M., Ledezma, M., and Hartman, C. (2013). “Shear resistance of tire-derived aggregate  
478 using large-scale direct shear tests. *Journal of Materials in Civil Engineering*. 04014110-1-8.

479 Xiao, M., Bowen, J., Graham, M., and Larralde, J. (2012). “Comparison of seismic responses of  
480 geosynthetically-reinforced walls with tire-derived aggregates and granular backfills.”  
481 *Journal of Materials in Civil Engineering*. 24(11), 1368-1377.

482 Youd, T. L. (1972). “Compaction of sands by repeated shear straining.” *Journal of Soil*  
483 *Mechanics and Foundations Division*, ASCE. 98(7), 709-725.

484

485 **Table 1:** Summary of previous studies involving the cyclic response of TDA (Note: damping  
 486 ratio and shear modulus values from Kaneko et al. (2003) and Hazarika et al. (2010)  
 487 reinterpreted from reported hysteresis loops)

<b>Test Parameters and Results</b>	<b>Feng and Sutterer (2000)</b>	<b>Kaneko et al. (2003)</b>	<b>Hazarika et al. (2010)</b>
Equipment type	Resonant column/ Torsional Shear	Cyclic simple shear	Cyclic triaxial
TDA type	Granulated rubber	Tire chips	Tire chips
TDA specific gravity	1.11	1.15	1.15
Specimen shape	Cylinder	Cylinder	Cylinder
Specimen diameter (mm)	70	60	50
Specimen height (mm)	150	40	100
Maximum TDA particle size (mm)	4.76	1.1	1.0
Saturation conditions	Dry	Saturated	Saturated
Confining stress range (kPa)	69-483	37.57-43.68	100
Cyclic strain range (%)	0.003-0.1	2.7-4.4	2.5
Damping ratio (%)	4.2-6.0	15.0-24.0	10.0
Shear modulus (kPa)	1100-2800	160-200	1484

488  
 489 **Table 2:** Summary of Type B TDA simple shear testing program  
 490  
 491

<b>Test</b>	<b>Shear Strain Amplitude (%)</b>	<b>Vertical Stress at Specimen Mid-Height, <math>\sigma_v</math> (kPa)</b>	<b>Initial Total Unit Weight (kN/m<sup>3</sup>)</b>	<b>Initial Void Ratio</b>
SS1	0.1, 0.3, 1, 3, 0.3, 1, 3, 10	19.3	5.64	1.00
SS2	0.1, 0.3, 1, 3, 10	38.3	6.59	0.71
SS3	0.1, 0.3, 1, 3, 10	57.5	6.82	0.65
SS4	0.1, 0.3, 1, 3, 10	76.6	7.07	0.60

492  
 493



494 **LIST OF FIGURE CAPTIONS**

495 **FIG. 1:** Large scale combination direct shear/simple shear device in simple shear mode:

496 (a) Schematic diagram; (b) Photograph

497 **FIG. 2:** Time histories for cyclic simple shear test SS1: (a) Horizontal displacement; (b) Shear

498 force; (c) Volumetric strain

499 **FIG. 3:** Time histories for cyclic simple shear test SS2: (a) Horizontal displacement; (b) Shear

500 force; (c) Volumetric strain

501 **FIG. 4:** Time histories for cyclic simple shear test SS3: (a) Horizontal displacement; (b) Shear

502 force; (c) Volumetric strain

503 **FIG. 5:** Time histories for cyclic simple shear test SS4: (a) Horizontal displacement; (b) Shear

504 force; (c) Volumetric strain

505 **FIG. 6:** Volumetric strain at the end of 20 cycles for each test stage

506 **FIG. 7:** Hysteresis loops for all cyclic shear strain amplitudes: (a) SS1, (b) SS2, (c) SS3; (d)

507 SS4

508 **FIG. 8:** Backbone curves corresponding to 20 cycles of loading at four vertical stress levels

509 **FIG. 9:** Normalized shear modulus and normalized damping ratio for test SS3

510 **FIG. 10:** Effect of cyclic shear strain amplitude on average values of: (a) Shear modulus; (b)

511 Damping ratio

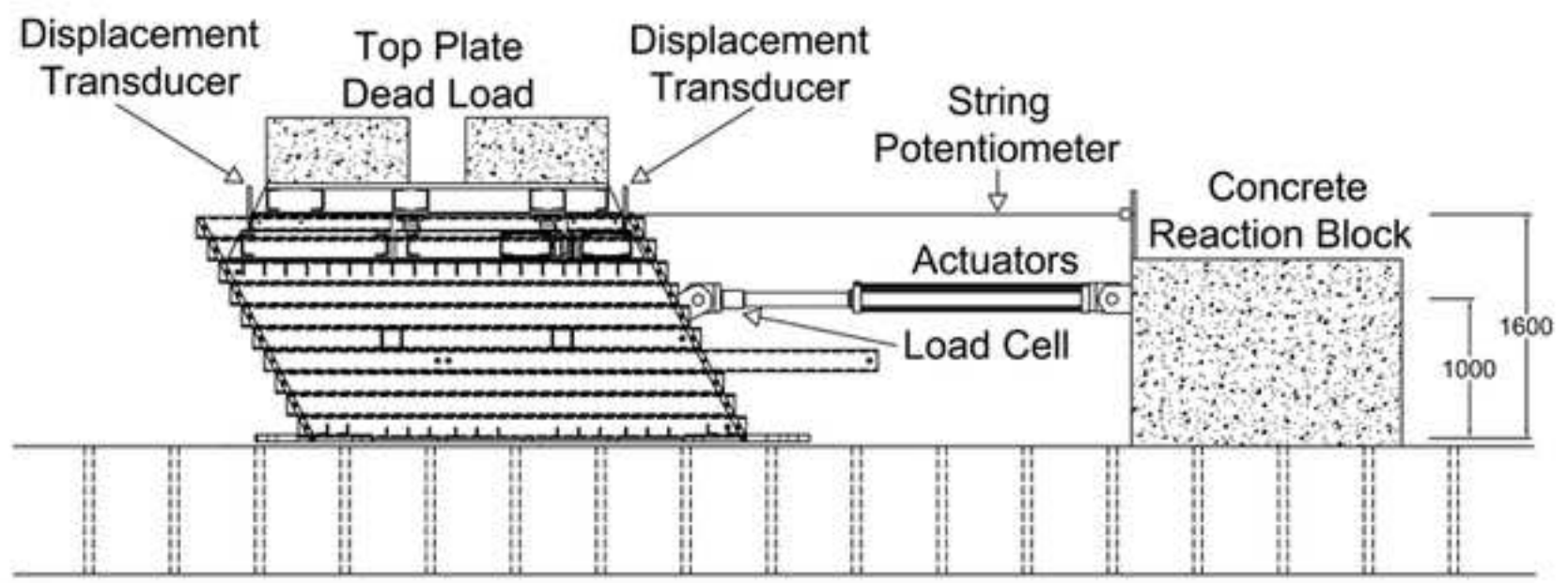
512 **FIG. 11:** First specimen and second specimen properties for test SS1: (a) Shear modulus;

513 (b) Damping ratio

514 **FIG. 12:** Effect of vertical stress and cyclic shear strain amplitude on shear modulus of Type B

515 TDA

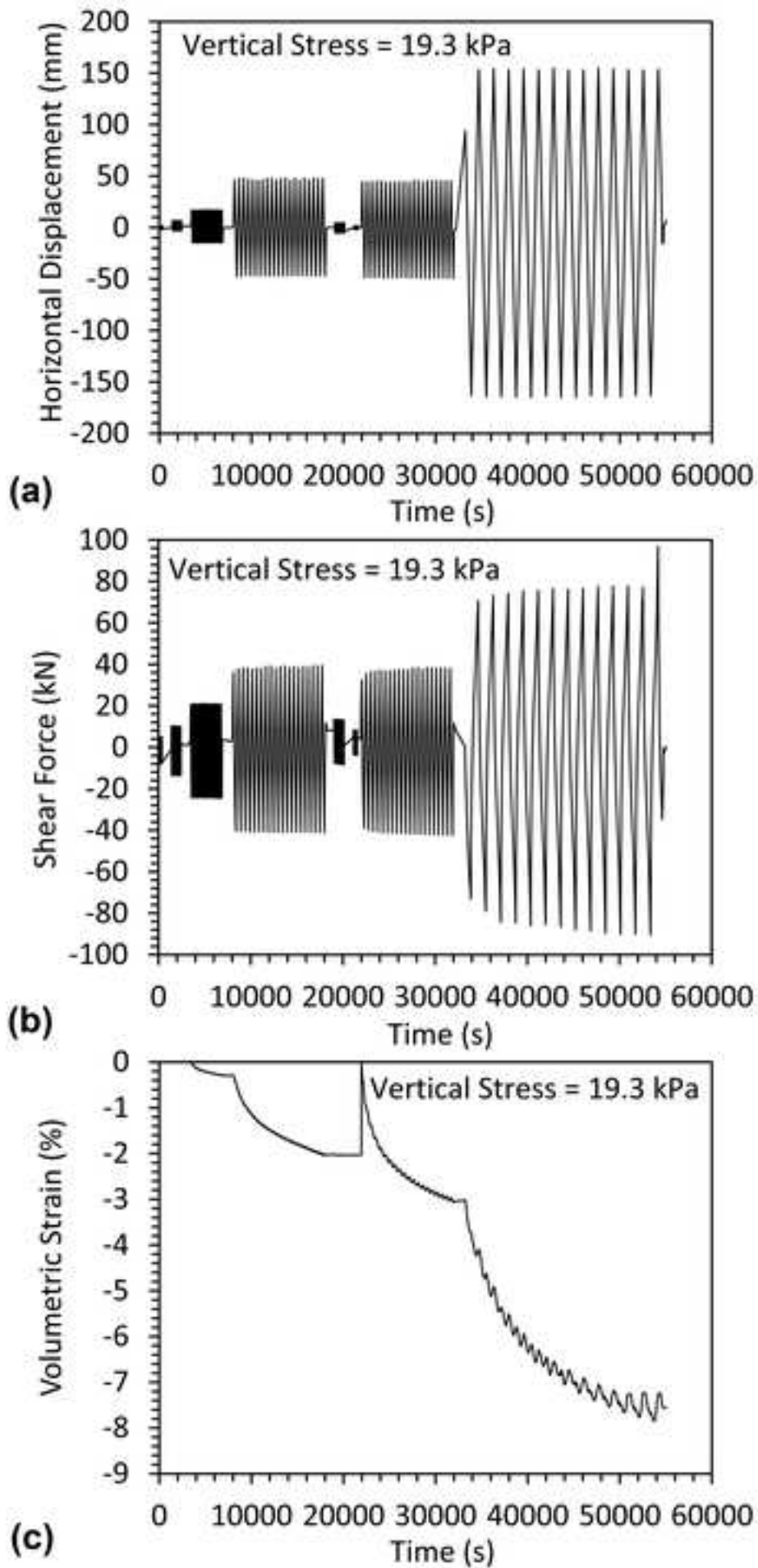
516 **FIG. 13:** Estimated shear modulus reduction curves for Type B TDA: (a)  $G$  vs.  $\gamma$ ,  
517 (b)  $G/G_{\max}$  vs.  $\gamma$

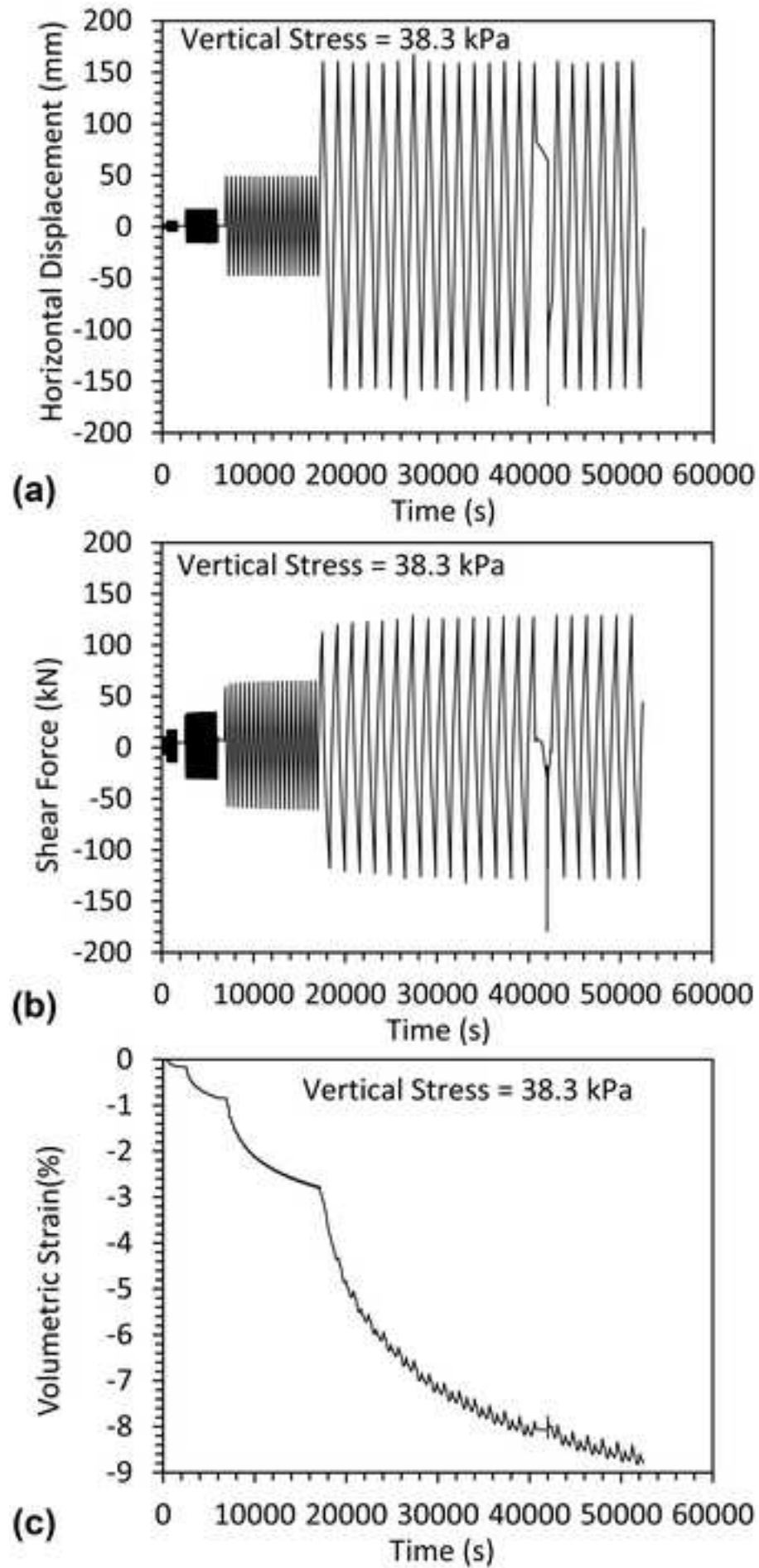


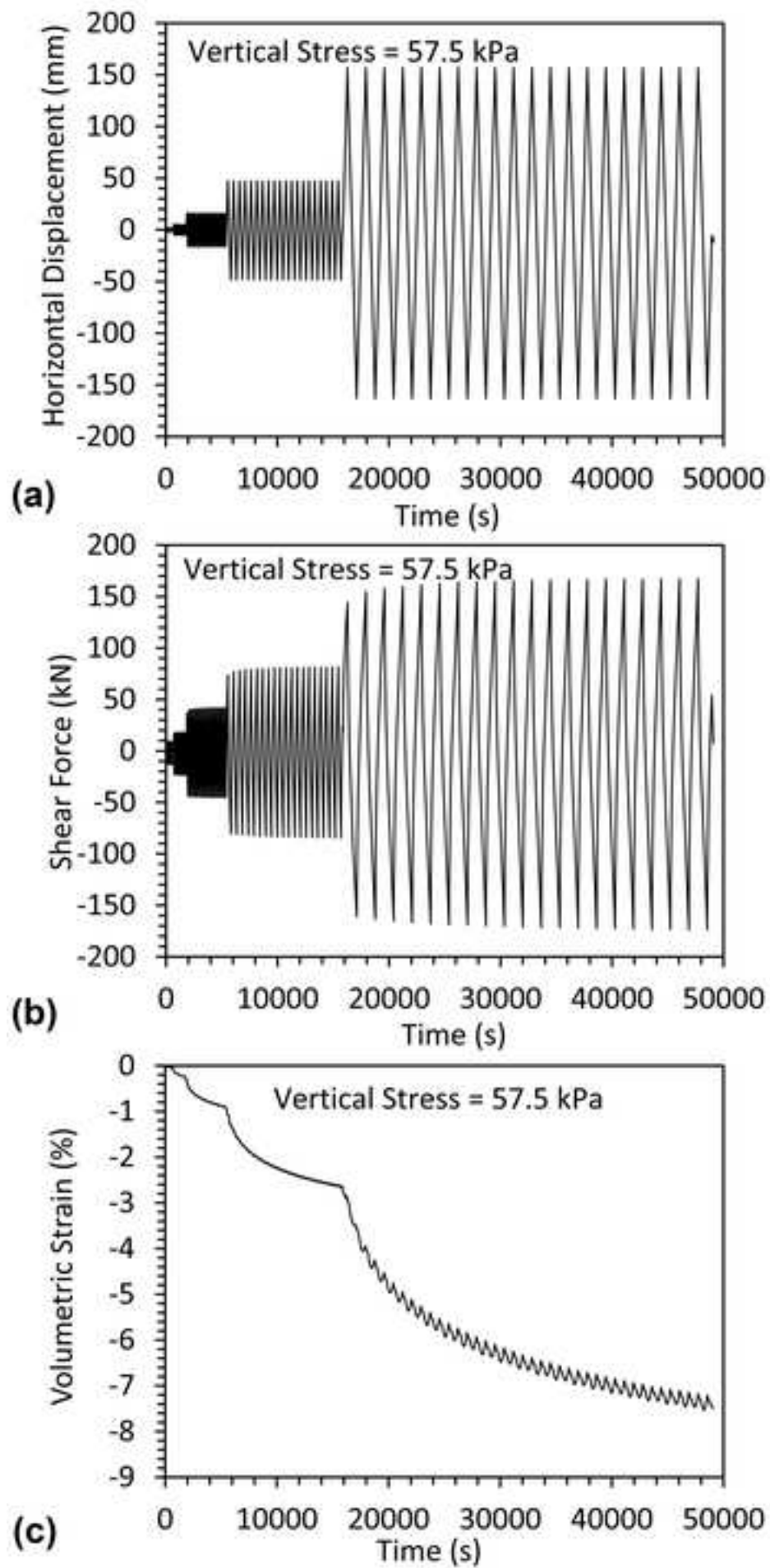
(a)

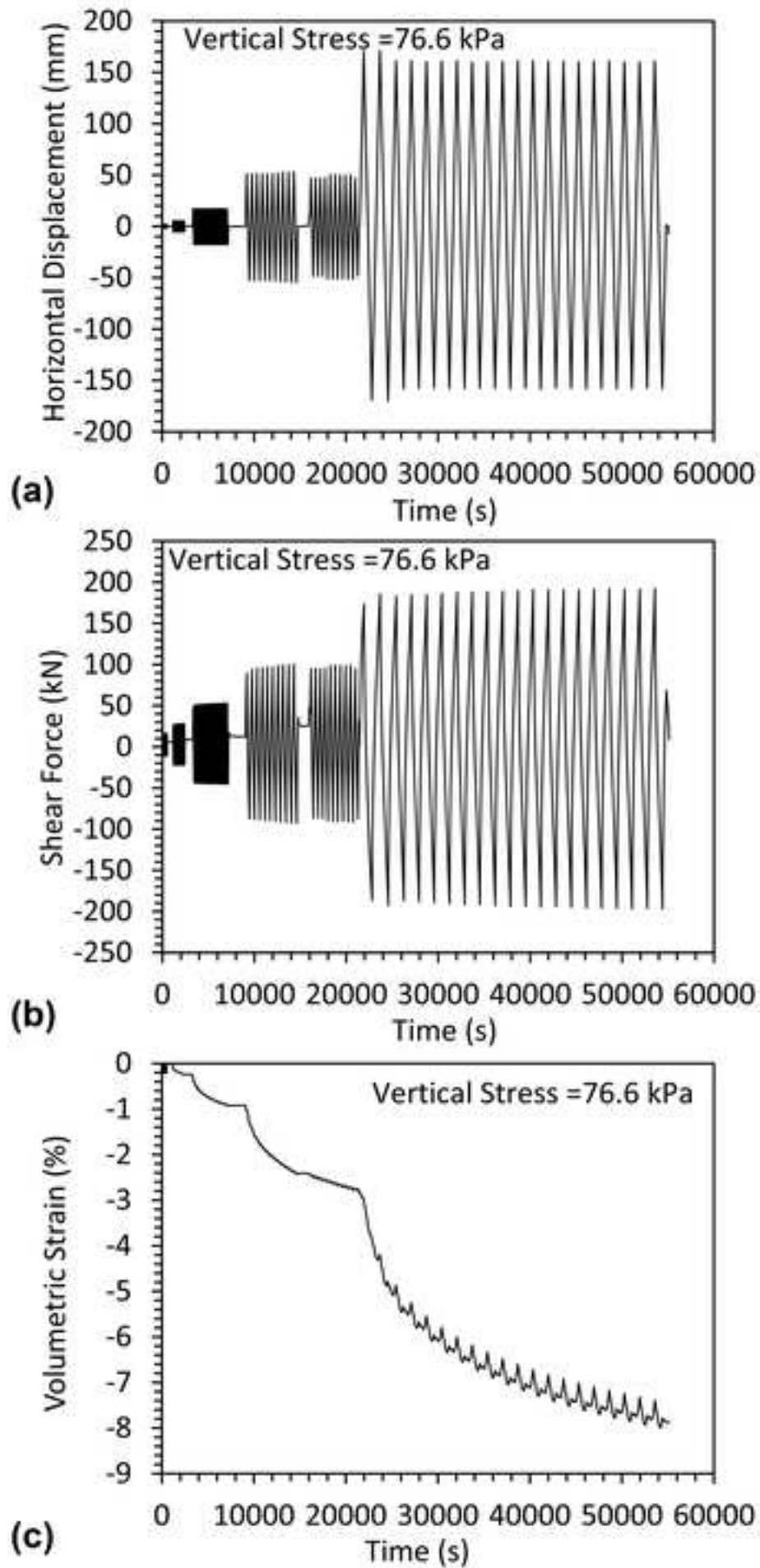


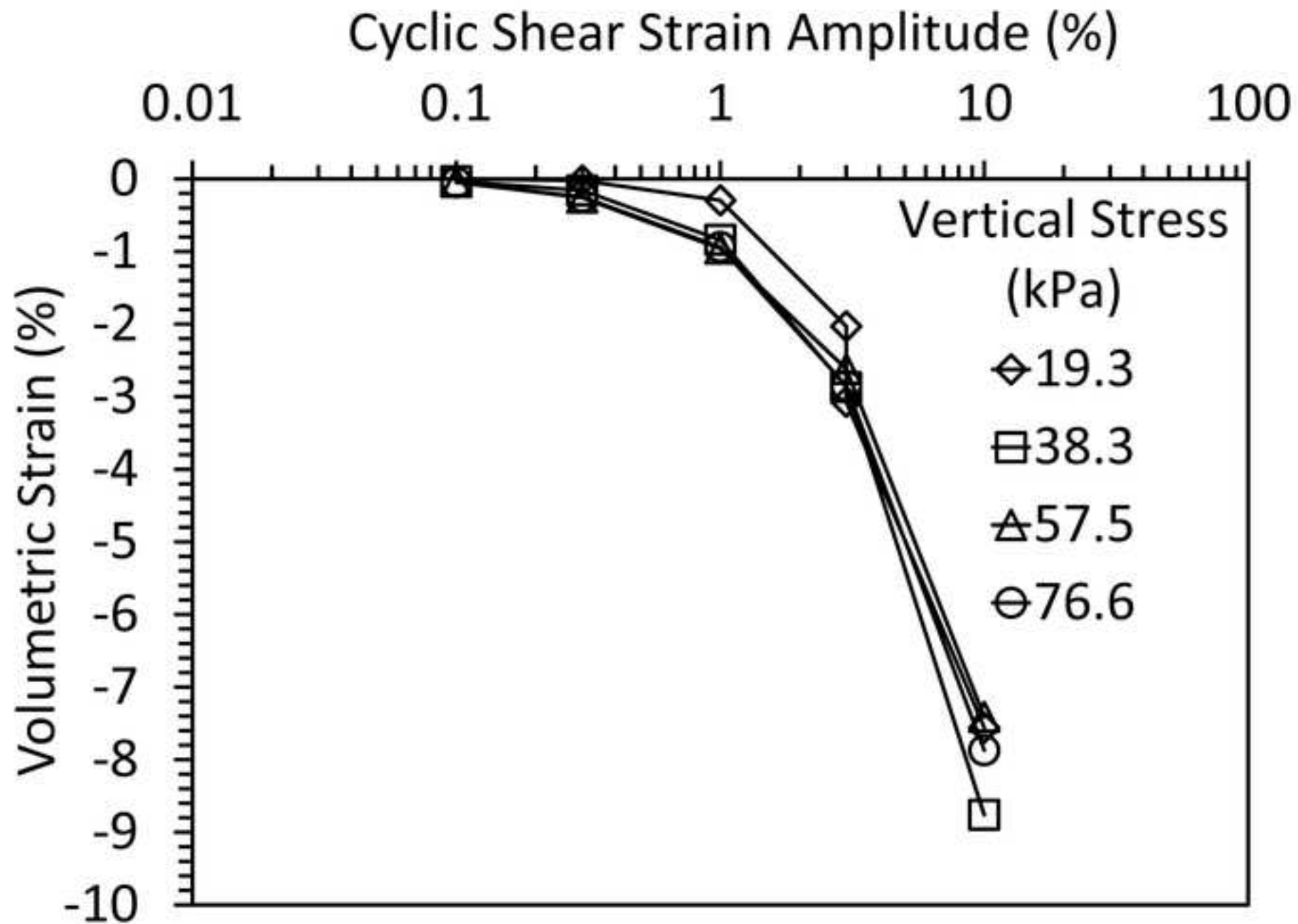
(b)



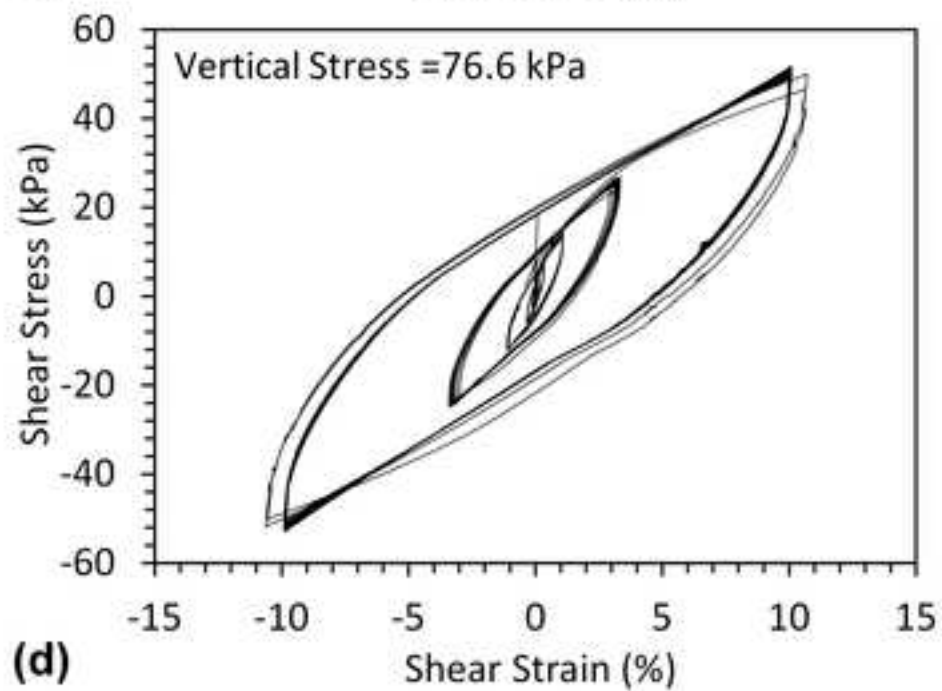
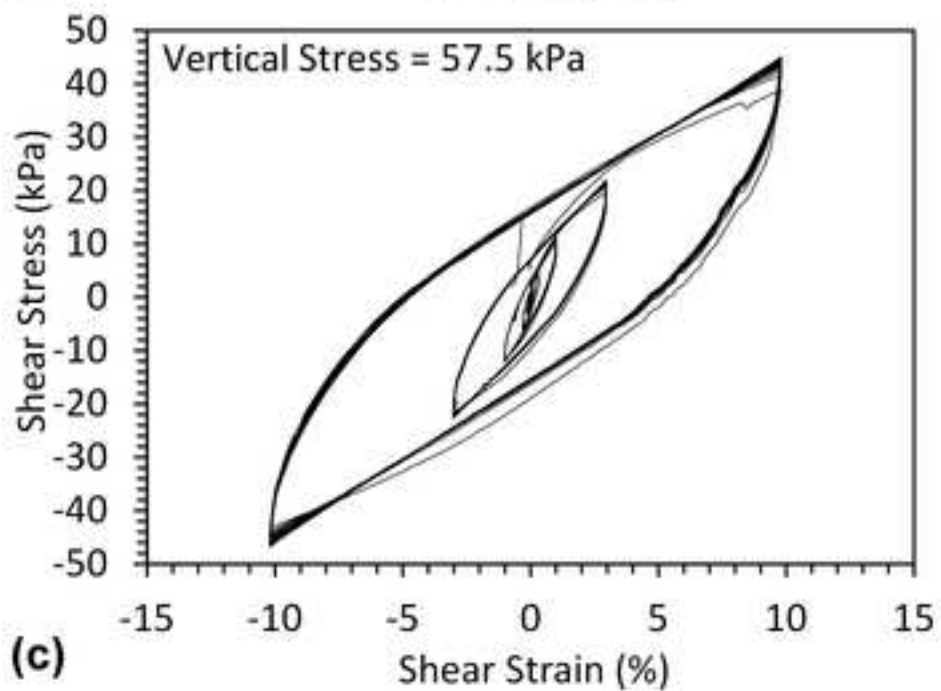
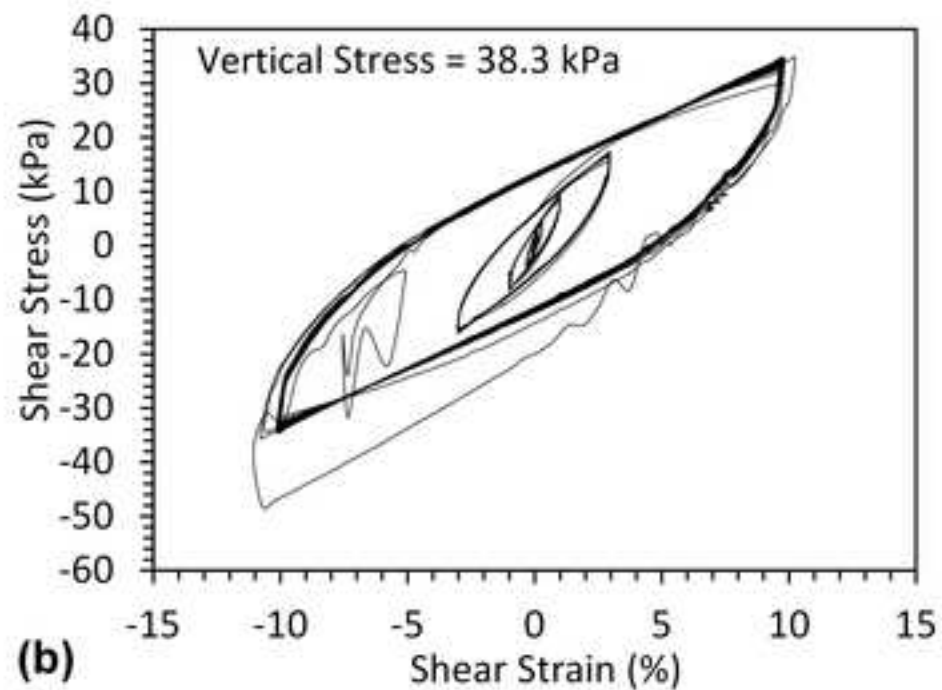
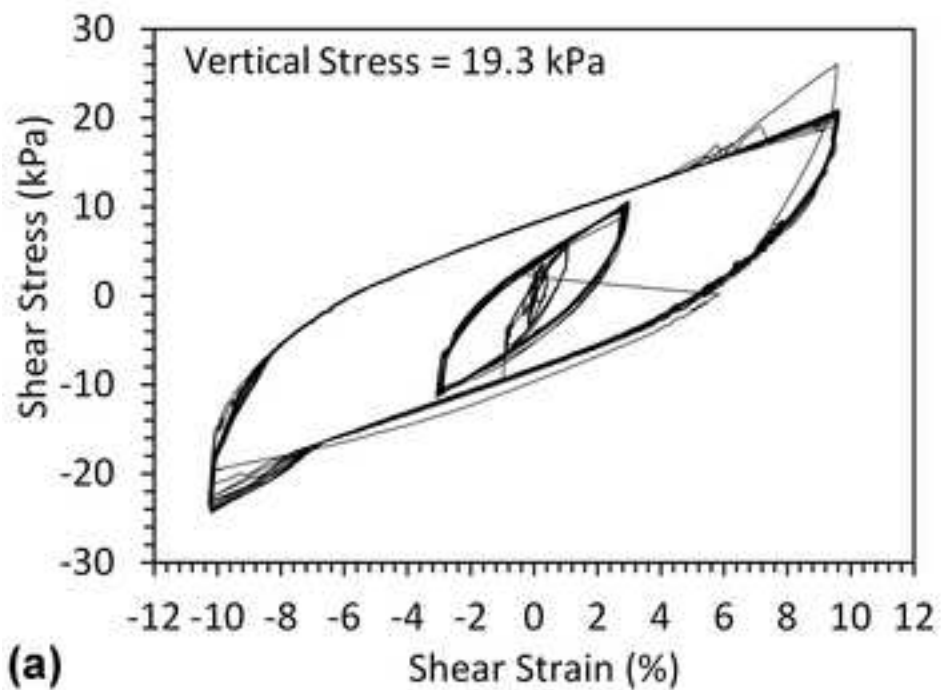


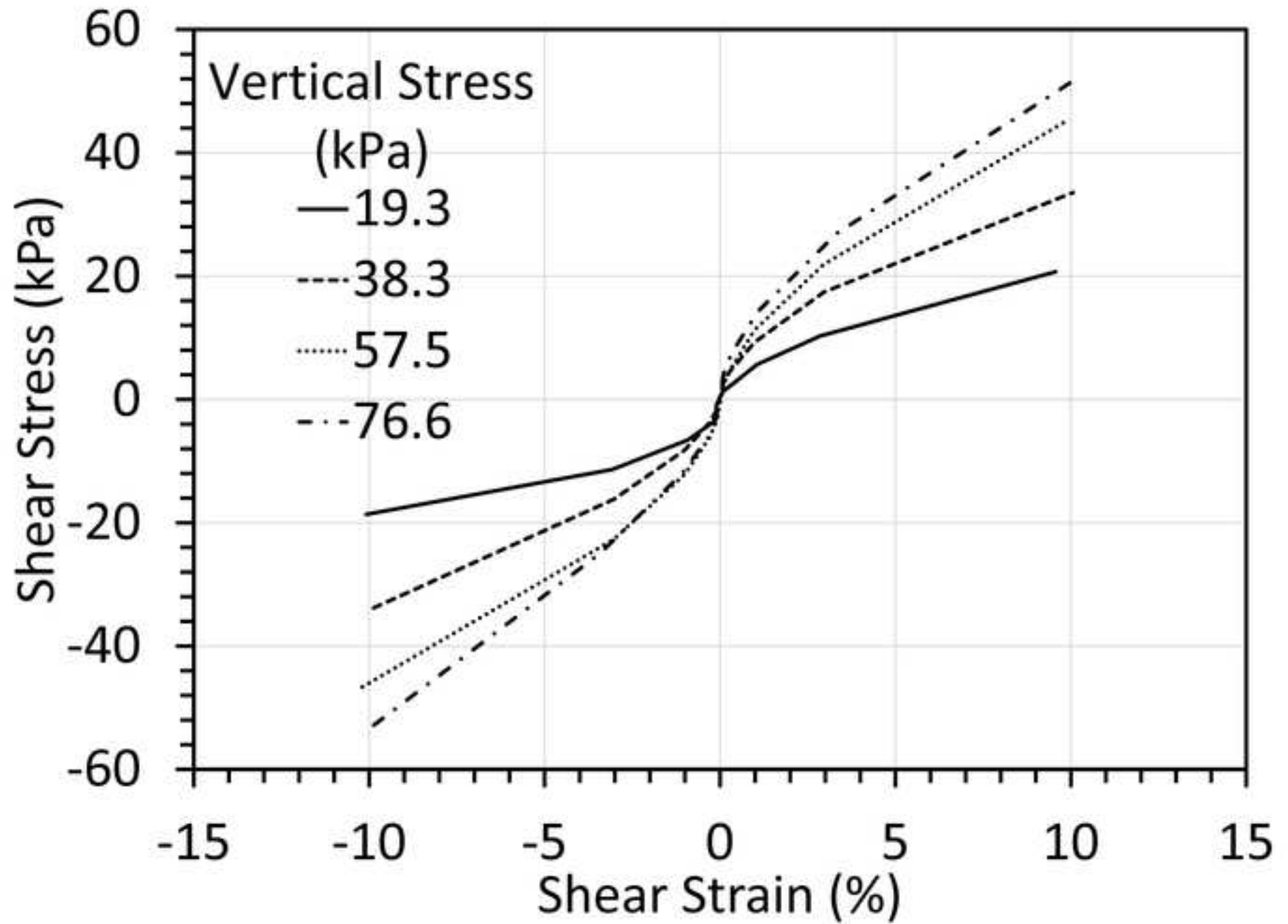


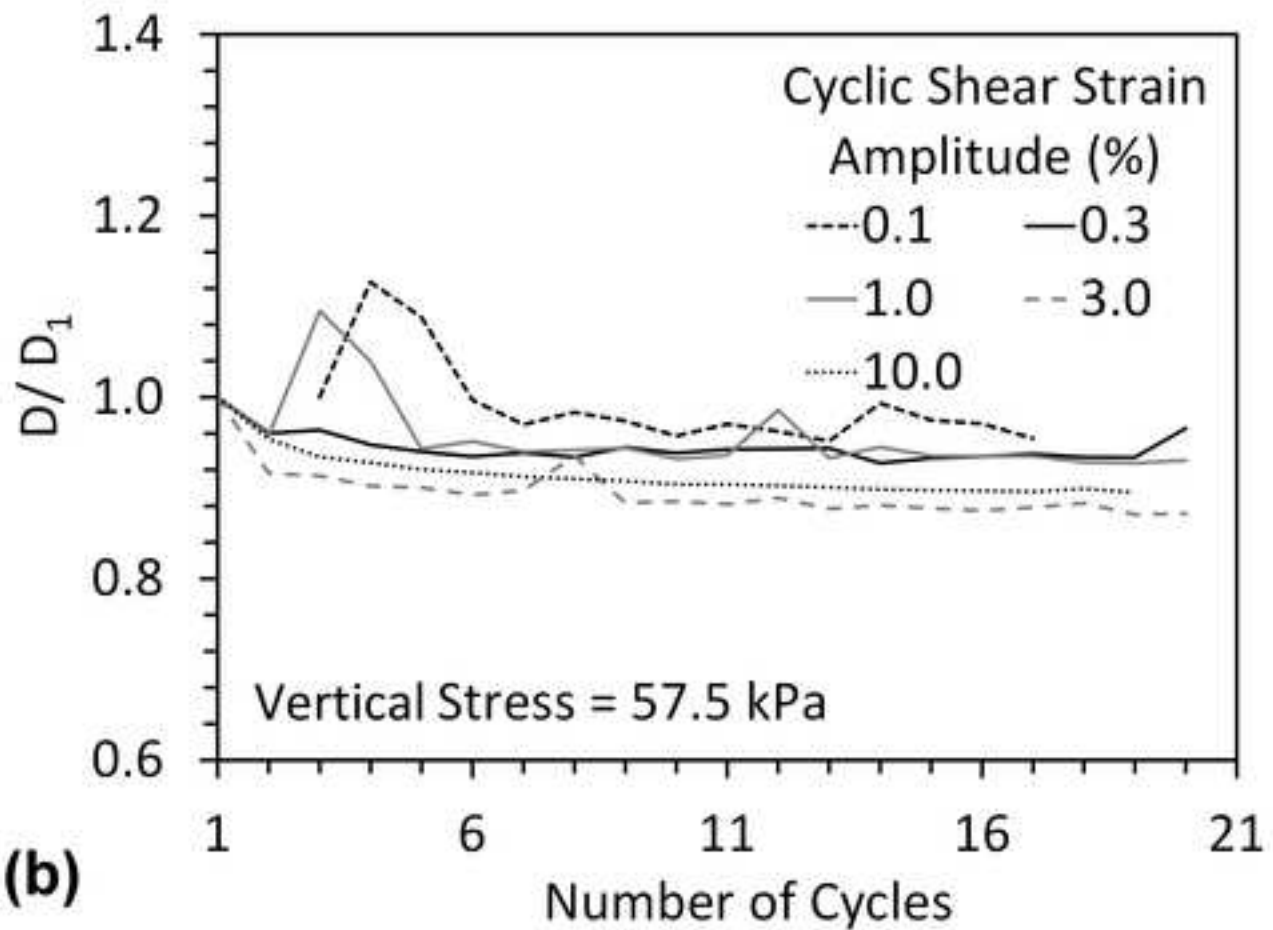
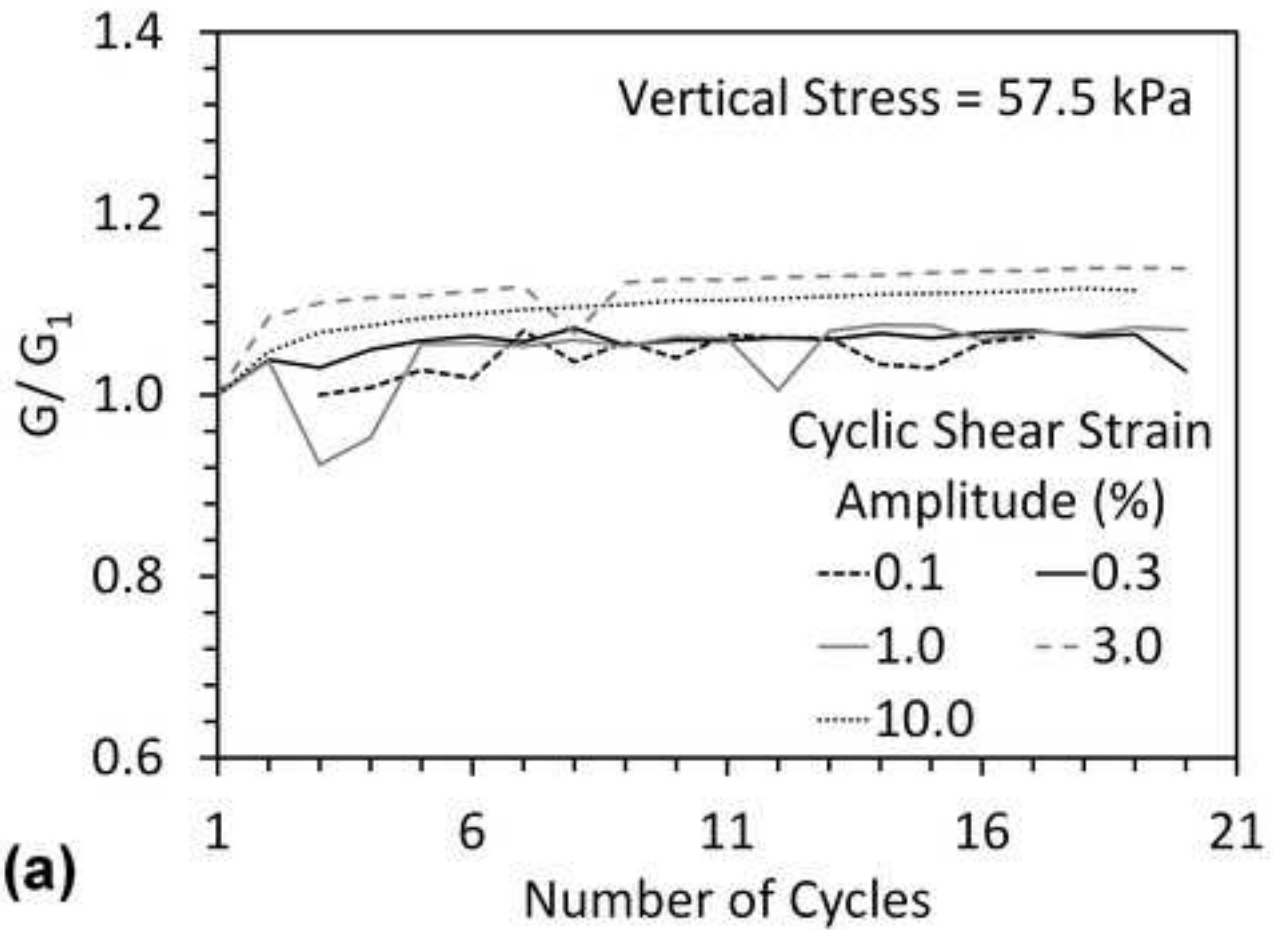


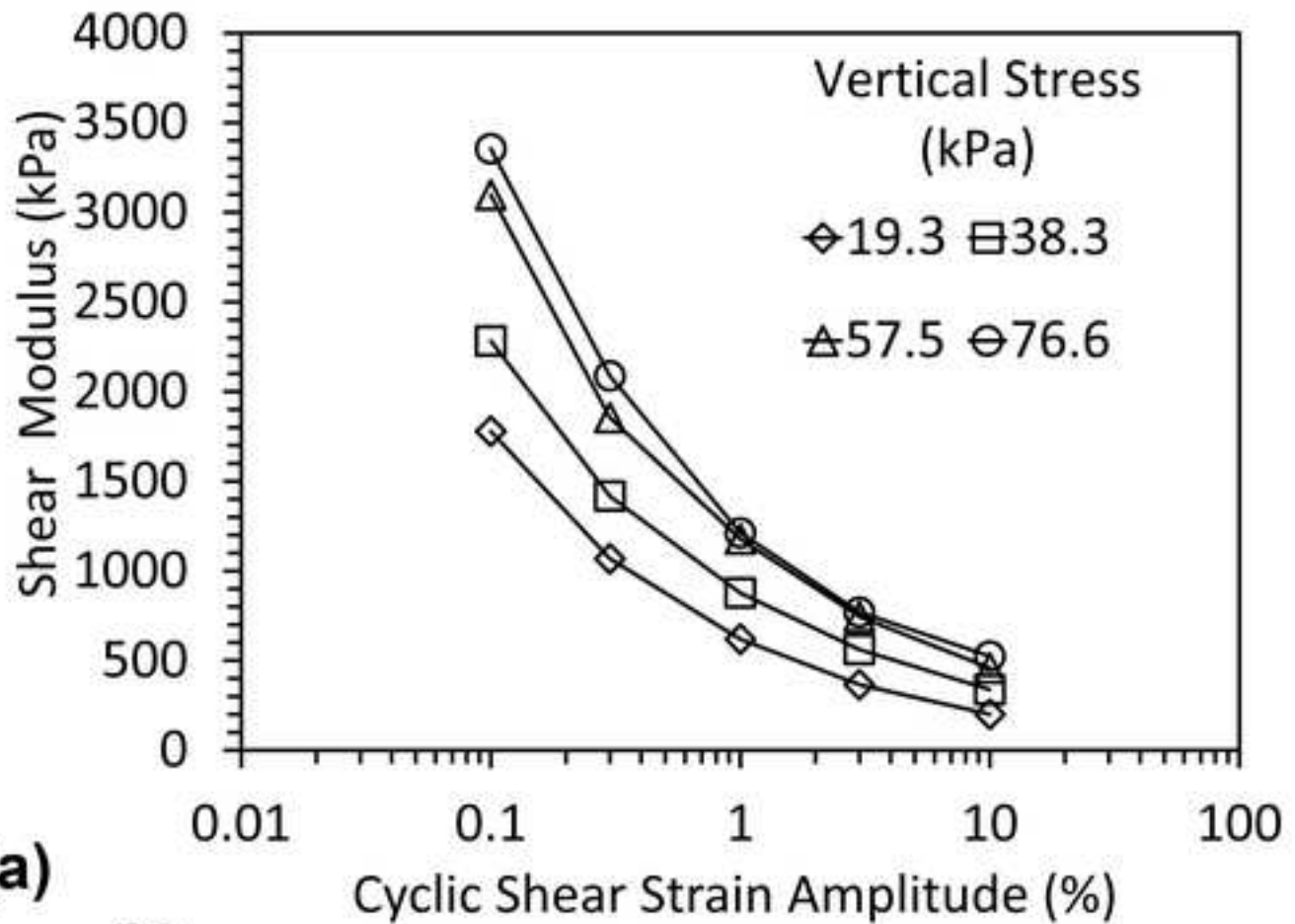




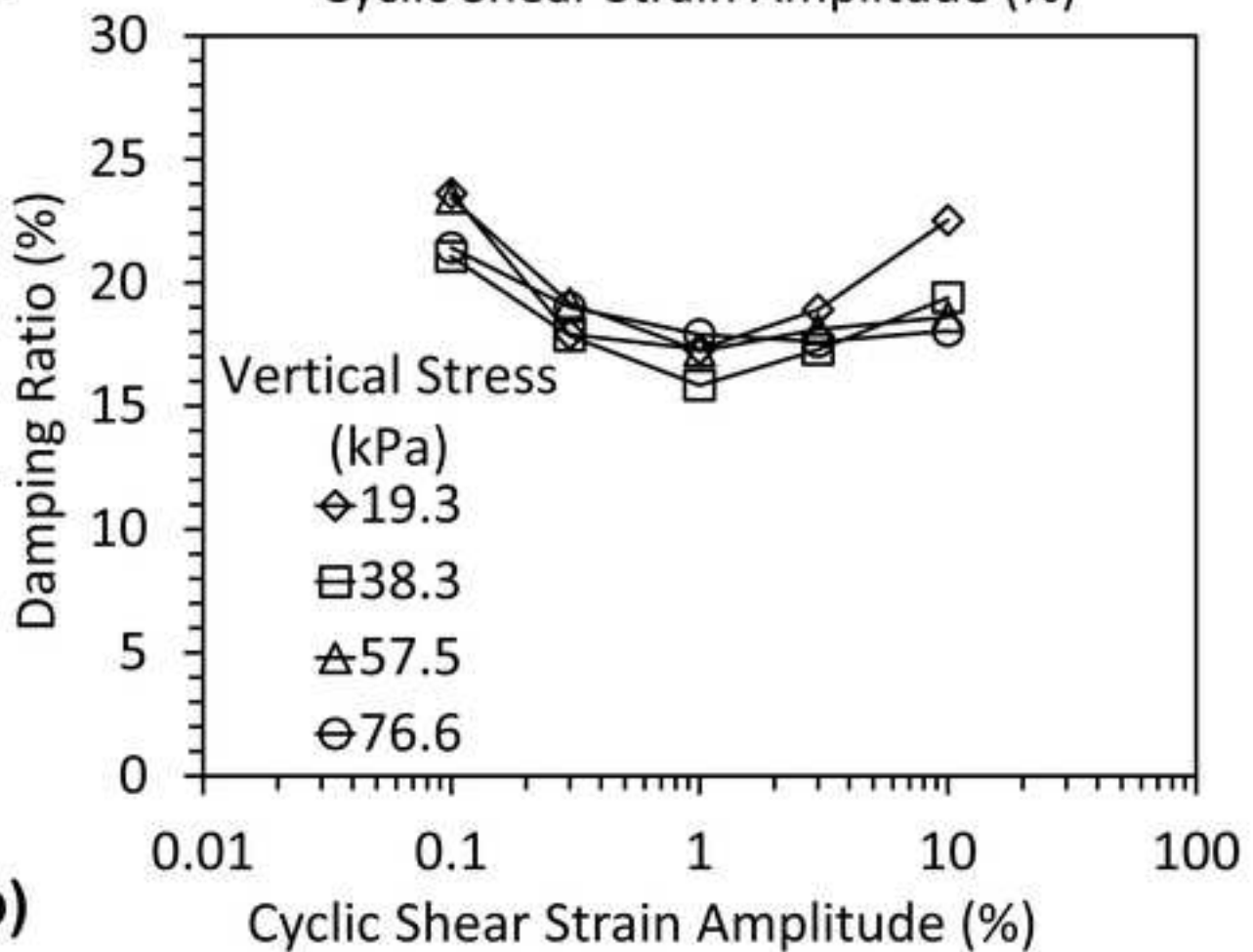




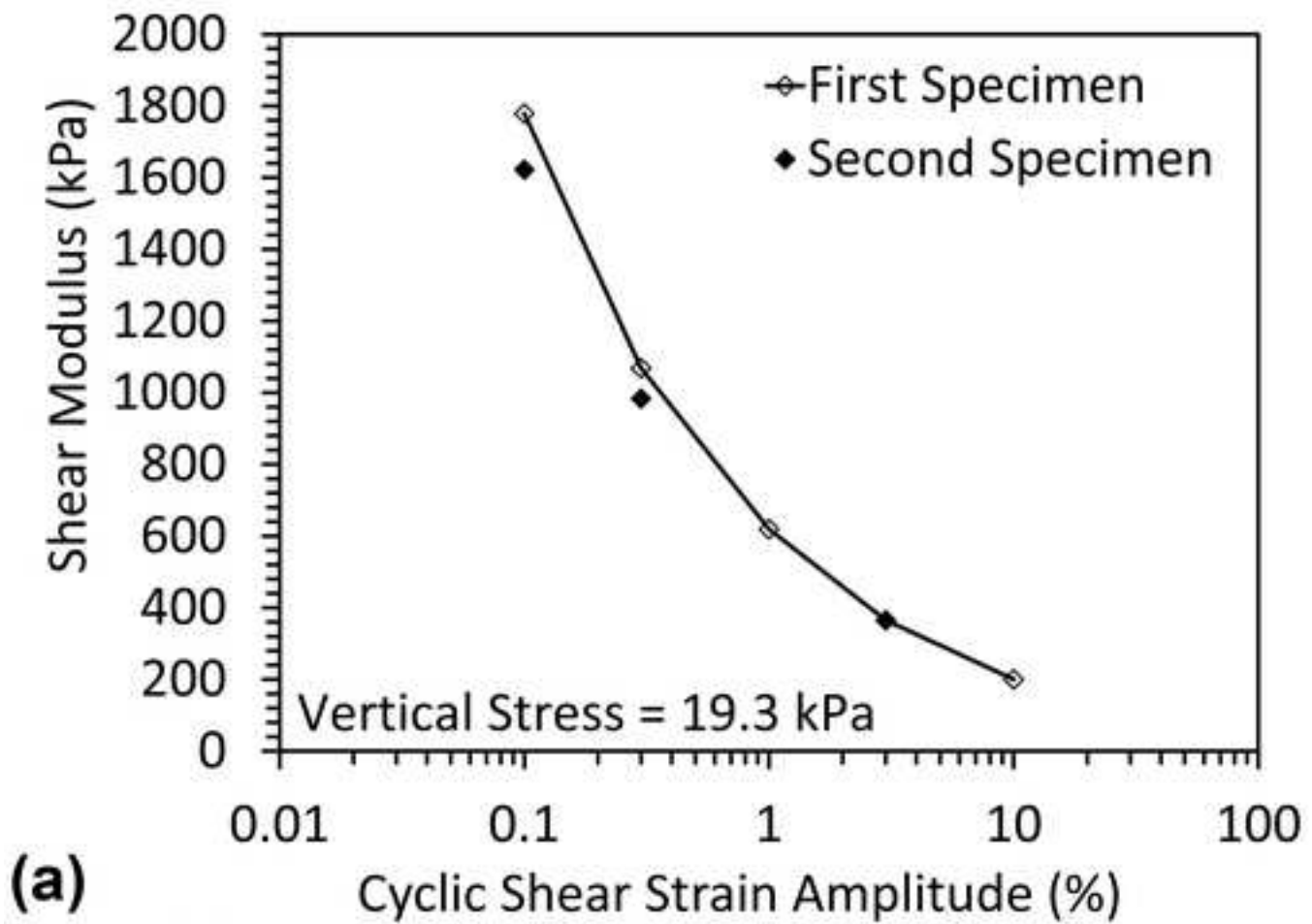
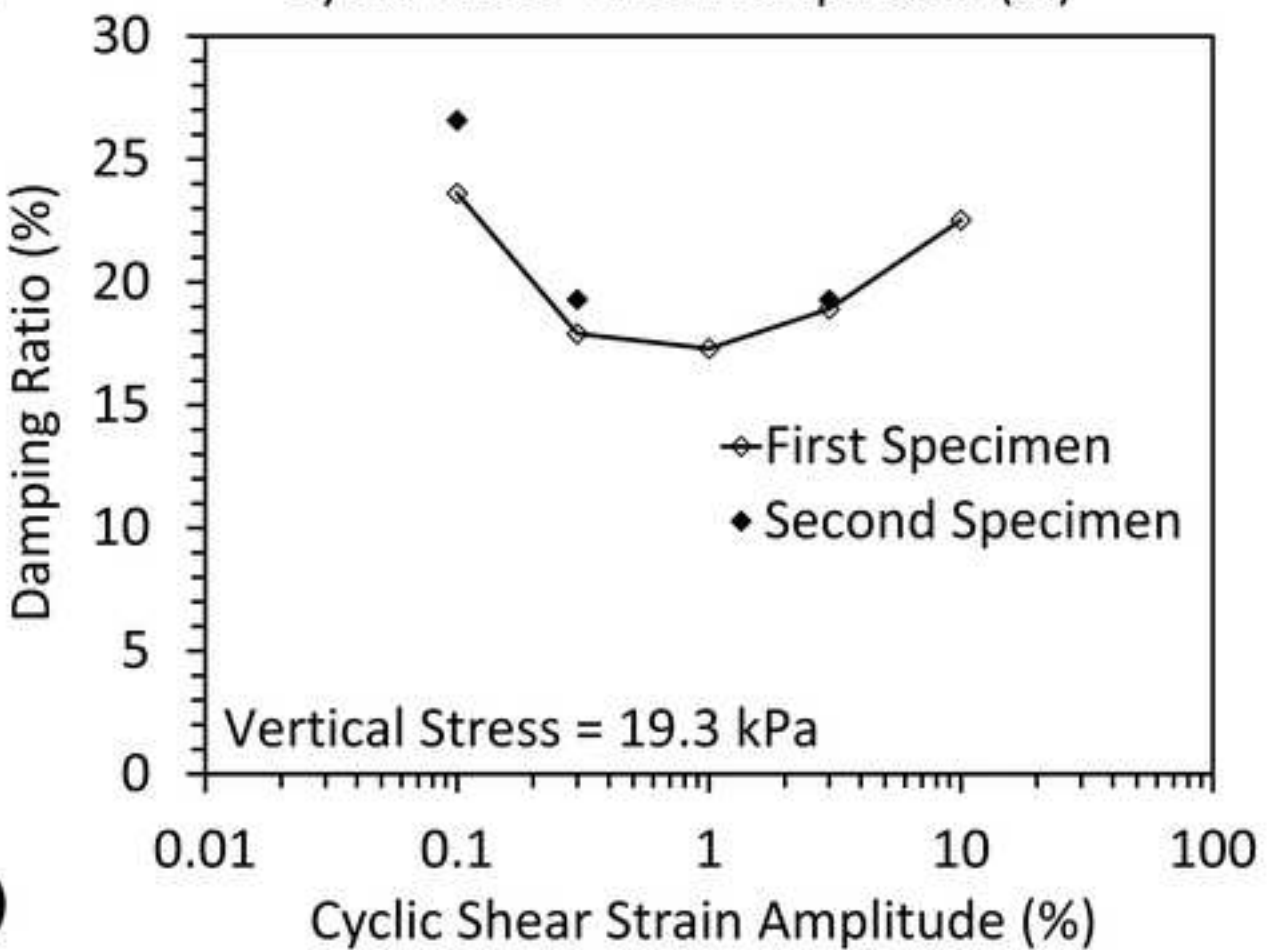


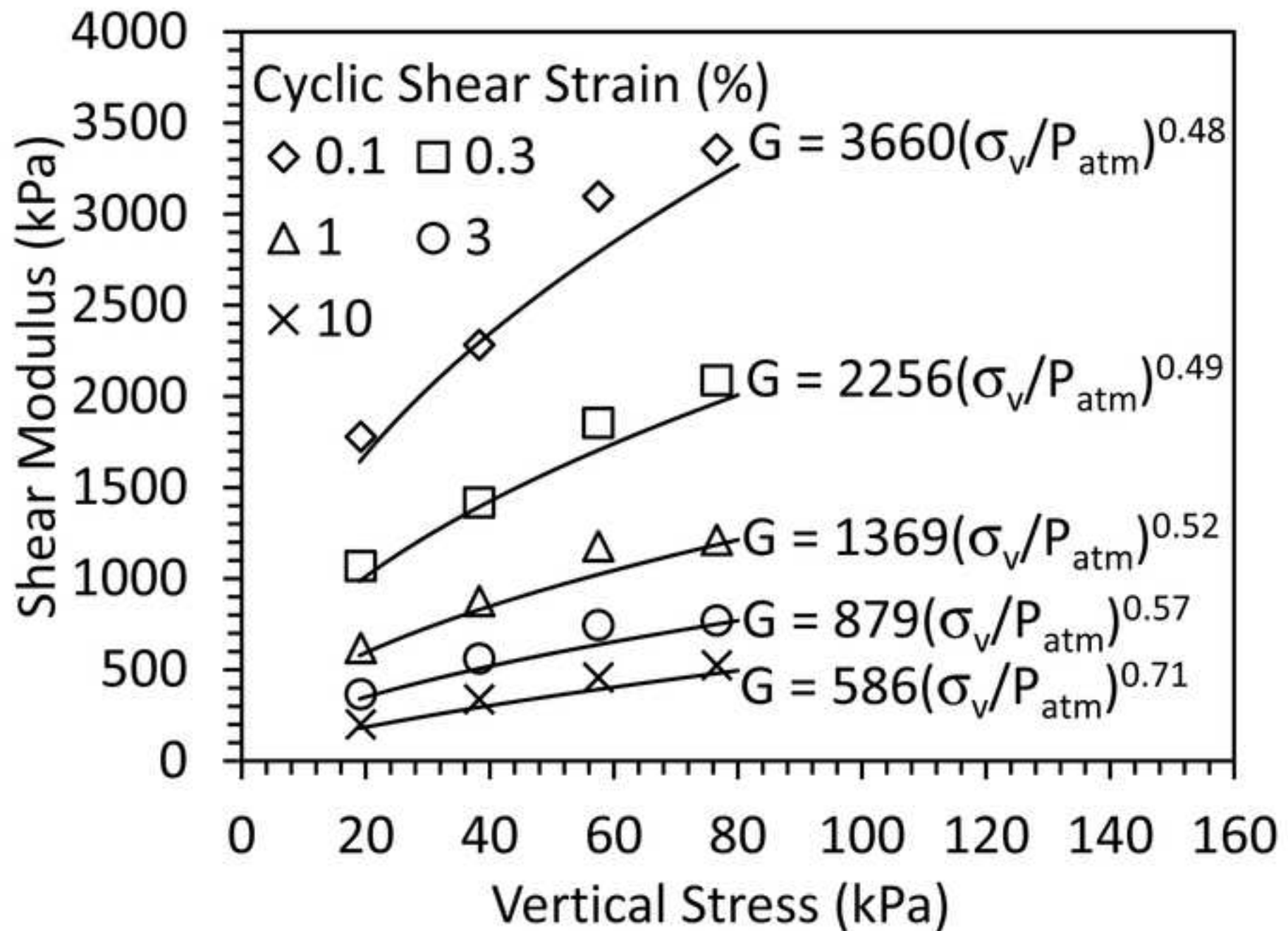


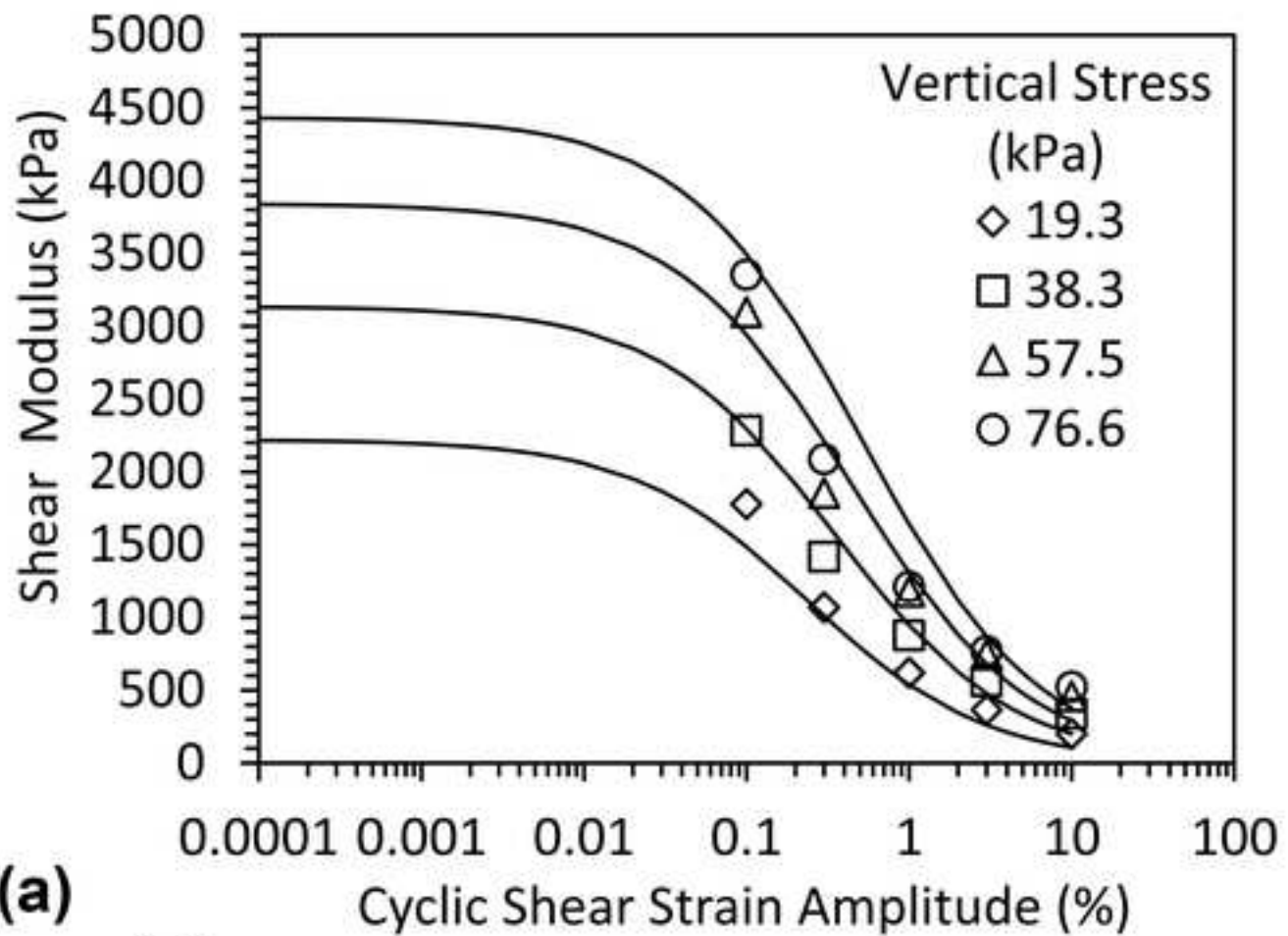
(a)



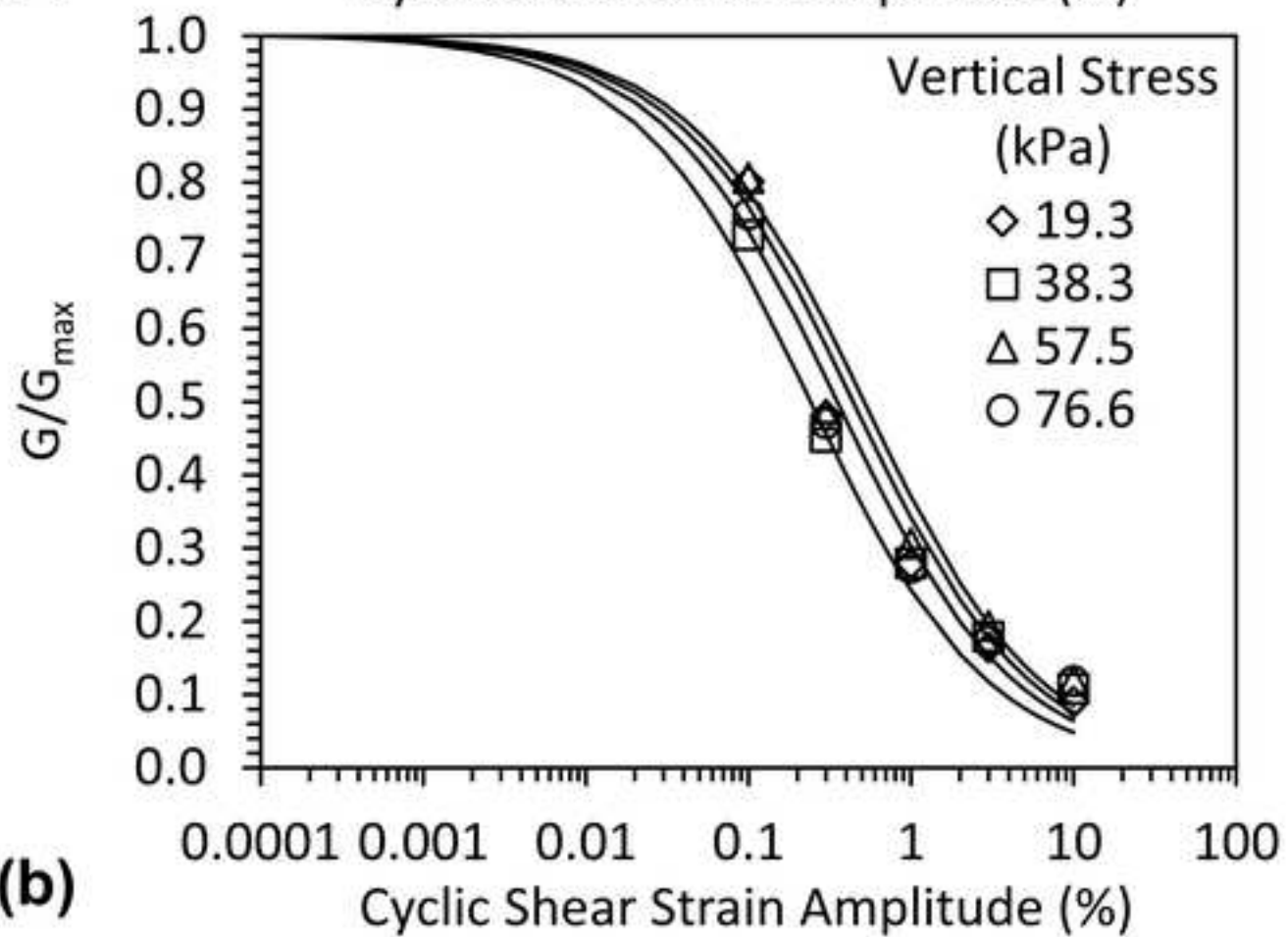
(b)

**(a)****(b)**





(a)



(b)